Global and Planetary Change 177 (2019) 10–26

Contents lists available at ScienceDirect

Global and Planetary Change

journal homepage: www.elsevier.com/locate/gloplacha

Comparison of climate change from Cenozoic surface uplift and glacial-interglacial episodes in the Himalaya-Tibet region: Insights from a regional climate model and proxy data

Heiko Paeth[a,*], Christian Steger[a,1], Jingmin Li[b,2], Felix Pollinger[a], Sebastian G. Mutz[b], Todd A. Ehlers[b]

[a] Institute of Geography and Geology, University of Würzburg, Germany
[b] Department of Geosciences, University of Tübingen, Germany

ARTICLE INFO

Keywords:
Tibetan Plateau
Dynamical downscaling
Paleo-climate
Surface uplift
Last glacial maximum
Mid-Holocene

ABSTRACT

Assessing paleo-climatic changes and the underlying driving mechanisms are an essential (and often poorly understood) first-step for understanding if natural variability in Earth's climate system from tectonic processes and orbital forcing could produce observed changes in surface processes. In this study, we take this first step of evaluating climate change in the Tibetan Plateau region for different distinct climate states. We do this using a high-resolution regional climate model parameterized for the Cenozoic rise of the Plateau and prominent Quaternary glacial and interglacial episodes. The main objective is to delimit the range of climate variability due to important natural drivers in the region by comparing climate changes during the main Cenozoic uplift period with climate anomalies during the last glacial maximum and the mid-Holocene optimum. This helps to interpret environmental changes documented by proxy data and to benchmark man-made climate changes expected during the 21st century. The innovative aspects of this study pertain to the use of a consistent high-resolution modeling framework and a multivariate statistical assessment of climate types and their shift during the various paleo-climatic episodes.

Reduced plateau elevation leads to regionally differentiated patterns of higher temperature and lower precipitation amounts on the plateau itself, whereas surrounding regions are subject to colder conditions. In particular, Central Asia receives much more precipitation prior to the uplift, mainly due to a shift of the stationary wave train over Eurasia. Cluster analysis indicates that the continental-desert type climate, which is widespread over Central Asia today, appears with the Tibetan Plateau reaching 50% of its present-day elevation.

The mid-Holocene is characterized by slightly colder temperatures, and the last glacial maximum by considerably colder conditions over most of central and southern Asia. Precipitation anomalies during these episodes are less pronounced and spatially heterogeneous over the Tibetan Plateau. The simulated changes are in good agreement with available paleo-climatic reconstructions from proxy data. The present-day climate classification is only slightly sensitive to the changed boundary conditions in the Quaternary. However, it is shown that in some regions of the Tibetan Plateau the climate anomalies during the Quaternary have been as strong as the changes occurring during the uplift period.

1. Introduction

The Tibetan Plateau (TP) is the highest and largest modern elevated plateau and a primary feature of Earth's climate system. Over the last millions of years it has experienced large climate change, especially during the Oligocene-Miocene-Pliocene uplift period (Clift and Plumb, 2008, Liebke et al., 2013, Clift et al., 2014) and in the interplay of glacial and interglacial epochs (Braconnot et al., 2012; Ruddiman, 2014). The TP represents a dominant driver of climate variability all around the globe (Molnar, 2005). In particular, the thermodynamic and mechanical effect of the TP on the strength, spatial extent and seasonal evolution of the South and East Asian monsoon systems makes it an

* Corresponding author at: Institute of Geography and Geology, University of Würzburg, Am Hubland, 97070 Würzburg, Germany.
E-mail address: heiko.paeth@uni-wuerzburg.de (H. Paeth).
[1] Now at: Deutscher Wetterdienst, Offenbach, Germany.
[2] Now at: German Aerospace Center, Oberpfaffenhofen, Germany.

https://doi.org/10.1016/j.gloplacha.2019.03.005
Received 11 July 2018; Received in revised form 1 March 2019; Accepted 12 March 2019
Available online 18 March 2019
0921-8181/

outstanding factor for low-frequency climate variations (Molnar and Rajagopalan, 2012; Park et al., 2012; Tang et al., 2013a). The TP is also a key region of investigation for the current debate on anthropogenic climate change. Climate reconstructions and meteorological data attest to increased warming rates and record high temperatures during recent decades in the TP region (Guo and Wang, 2012; Guangliang et al., 2013) and climate model projections identify one of the hot spots of future climate change in the mountainous areas of Central Asia (Yang et al., 2012; IPCC, 2013; Mannig et al., 2013).

The assessment of the anthropogenic interference with climate and its relevance for ecosystems and society requires that the magnitude of natural climate variations and their underlying mechanisms are well understood (e.g. Ruddiman, 2014). Given this, this study is dedicated to several outstanding paleo-climatic episodes that we compare in a consistent modeling framework in high spatial resolution. A number of sensitivity studies with a high-resolution regional climate model (RCM) are presented to simulate climate equilibrium states: (1) during different stages of surface uplift of the TP, (2) during the last glacial maximum (LGM), and (3) during the mid-Holocene (MH) climate optimum. These episodes have been identified as major time slices of paleo-climatic variability in the TP region and are also in the focus of proxy data retrieval and interpretation (e.g. Braconnot et al., 2012, Mielke et al. 2013, Clift et al., 2014, Ruddiman, 2014).

In this study, we complement previous work with a focus on two objectives that can be dealt with by means of the same experimental framework: the first objective of our study refers to the hypothesis that glacial versus interglacial orbital forcing conditions during the Quaternary can produce climate anomalies across the TP that are in the same order of magnitude as during Cenozoic (last ~55 Ma) surface uplift (cf. Prell and Kutzbach, 1992). This question is dedicated to a better process understanding of natural climate and environmental variations in one of the Earth's key regions of climate variability and change. For this purpose, we compare different episodes that relate to fundamentally different mechanisms and time scales of natural climate variability, for the first time by means of a coherent experimental design based on global and regional climate models.

Our second objective pertains to the generation of fine-scale patterns of paleo-climate for the TP and surrounding regions by relying on a high-resolution RCM. This is motivated by the fact that paleo-climatic episodes are derived from the interpretation of proxy-data based on tree rings, sedimentary archives, and stable isotope methods that are representative of local to regional rather than large-scale environmental conditions, especially in the mountainous regions of Central Asia (Bartlein et al., 2011; Grießinger et al., 2011; Bershaw et al., 2012; Mischke et al., 2013; Saraswat et al., 2013). Thus, higher-resolution simulated paleo-climatic patterns may bare more similarities with proxy-data. Here, we produce simulated climate equilibrium states, prescribing the specific boundary conditions for the various paleo-climatic episodes, which serve as a theoretical basis and benchmark for the interpretation of proxy-data. In addition, some episodes during the early uplift period are addressed where proxy-data are rarely available (Clift and Plumb, 2008).

2. Background and previous related work

The effect of the TP uplift on local and regional climate, with particular focus on the Indian summer monsoon, was investigated in earlier work (Hahn and Manabe, 1975), revealing the general relationship between uplift and cooling and drying on the TP as well as a strengthening of the South and East Asian monsoons (cf. Kutzbach et al., 1989, 1993). Since then, these basic mechanisms and climate responses have been corroborated by a number of modeling studies with global models using increasing resolution and complexity (e.g. Kitoh et al., 2010, Molnar and Rajagopalan, 2012, Park et al., 2012, Wu et al., 2012, Botsyun et al., 2016; Mutz et al., 2018). Recently, Ma et al. (2014) have demonstrated that the elevation of the Himalaya is more relevant to the changing climate patterns in the Asian monsoon regions than the height of the TP itself. Zhang et al. (2014) have prescribed several regionally differentiated uplift scenarios and draw a rather heterogeneous picture of the climate response to surface uplift. Common to these studies is that they are based on coarse-grid climate models which, probably, cannot account for the finer-scale characteristics of lower atmospheric circulation, precipitation and height-dependent temperature (Braconnot et al., 2012) in orographic terrain. The deficits of state-of-the-art global climate models for the assessment of present-day climate on the TP have been highlighted by Su et al. (2013). Harrison et al. (2014) have compared paleo-climatological simulations from various climate models with available proxy-data and pointed to a number of substantial biases over Asia. Kitoh et al. (2010) reported some added value when they enhanced the model horizontal resolution of their uplift experiments to 120 km. Finally, work by Botsyun et al. (2016) applied an isotope tracking global general circulation model (LMDZ-iso) to investigate the effect of surface uplift on precipitation $\delta^{18}O$. They document significant change in the isotopic composition of precipitation during surface uplift, and estimate only ~40% of existing stable isotope based paleo-altimetry sample locations contain a signal of the plateau surface uplift history. The work of Botysun et al. (2016) highlights the importance of paleoclimate modeling studies for understanding the tectonic, surface uplift, history of large orogenic plateaus.

As a consequence, RCMs have also been applied to paleo-climatological issues associated with plateau surface uplift over the Andes (e.g., Ehlers and Poulsen, 2009; Poulsen et al., 2010; Insel et al., 2010) and for the TP and Asian monsoon regions. For example, Zheng et al. (2004) have addressed the MH period for the TP at a resolution of 120 km. The LGM and MH have been compared by Ju and Jiang (2007) who revealed an added value of their RCM at 60 km resolution with respect to the driving global model. A similar result was obtained by Polanski et al. (2012) at 50 km resolution for the MH episode. Liu et al. (2008a, 2008b) have used an RCM with a lower resolution of 90 km but accounted for a large number of individual and combined forcings, indicating that changing vegetation, sea level and large-scale atmospheric circulation play a more important role in glacial climate than greenhouse gas concentrations and orbital parameters. In terms of the surface uplift process, Song et al. (2009) have carried out a sequence of experiments with stepwise elevation increase but restricted their simulation period to several months only. More recent RCM simulations with low resolution but spatially differentiated uplift scenarios highlighted the crucial importance of the Himalayan barrier effect for the Indian monsoon and the predominating impact of the TP elevation on the East Asian monsoon system (Tang et al., 2013a), whereas interannual monsoon variability is hardly affected by the uplift stages (Tang et al., 2013b).

In order to meet our main objectives and underlying hypotheses, we pursue a dynamical downscaling approach nesting the RCM REMO at 0.5° (~55 km) resolution into the global climate model ECHAM5 (Li et al., 2016, 2017; Mutz et al., 2016). For all paleo-climatic episodes the same model setup is used in terms of domain, resolution, model physics and driving model, albeit with different boundary conditions for surface uplift magnitude as well as LGM and MH environments (see Section 2). This approach allows for a direct comparison of the resulting climate anomalies with each other and for the assessment of extreme states in the course of natural climate fluctuations since the middle Tertiary. The climate modeling work presented here is part of the interdisciplinary joint research project 'Tibetan Plateau: Formation - Climate - Ecosystems' that is dedicated to environmental changes in the TP region during the last 70 million years and the upcoming role of mankind during recent millennia.

The subsequent section is dedicated to the description of the model, the experimental design, the validation data and the statistical methods. The results of our analysis are presented in Section 4 and discussed in Section 5. The last section comprises the main conclusions

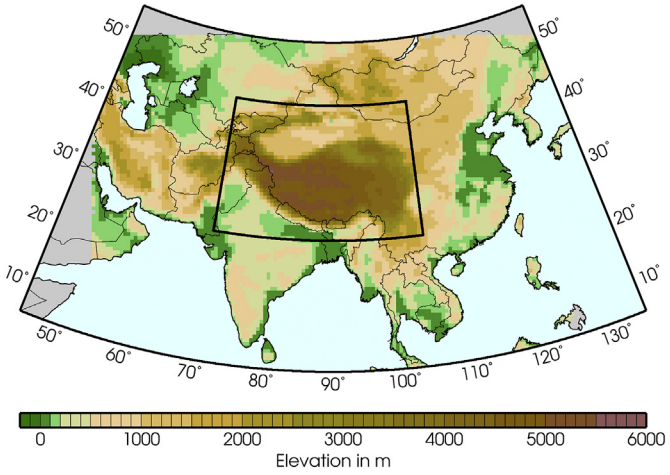

Fig. 1. Domain for the dynamical downscaling with REMO (outer region) and for the cluster analysis centered over the Tibetan Plateau (inner region).

and a brief outlook.

3. Modeling design, data and methods

The dynamical downscaling is undertaken with the hydrostatic RCM REMO (Jacob, 2001). It is nested in the atmospheric global climate model ECHAM5 which is the atmospheric part of the Max-Planck Institute for Meteorology coupled general circulation model ECHAM5/MPI-OM (Jungclaus et al., 2006), providing the lateral atmospheric and lower oceanic boundary conditions. For all paleo-climatic episodes REMO is run over the same model domain, extending from 50°E to 130°E and from the equator to 60°N (see Fig. 1). In addition, the same horizontal and vertical resolution is used, amounting to 0.5° and 27 levels, respectively. The current REMO version is based on the improved land surface scheme from Hagemann and Dümenil Gates (2003). In order to avoid misinterpretation due to lateral boundary effects of the nesting approach, the lateral eight grid box rows, i.e. a width of about 440 km, are excluded from data visualization and analysis.

REMO has been successfully applied and evaluated for climatological issues in Europe (Jacob, 2001), Africa (Paeth et al., 2005, 2009), South East Asia (Saeed et al., 2011) and Central Asia (Mannig et al., 2013). In the paleo-climatological context, it has been used in a former version with stable isotopes for uplift scenarios in the Andean region (Insel et al., 2012). Paxian et al. (2015) have recently identified an added value of REMO and other RCMs when it comes to decadal predictability in the West African monsoon system. In the present study, REMO is applied for the first time to a paleo-climatological problem in Asia, assuming that it represents a valuable and efficient tool to generate high-resolution patterns of paleo-climatic episodes to be compared with proxy- data. The REMO setup used here has been extensively evaluated by means of a number of sensitivity studies. Two types of experiments have been performed that are described below.

The first type of REMO experiments addresses the uplift process of the TP. For this purpose, the RCM in 0.5° resolution is nested into AMIP-type global simulations with ECHAM5 using a horizontal spectral resolution of T63 (~1.875°), 19 vertical levels and observed sea surface temperature and sea ice data from GISST (Rayner et al., 1996). The uplift is accounted for by a stepwise approach, setting the model topography in ECHAM5 and REMO to 100%, 75%, 50%, 25% and 0% of the present-day elevation. According to current geological knowledge (e.g. Molnar, 2005, Mielke et al. 2013, Clift et al., 2014), the topography is modified in the domain indicated by the red line in the top panel of Fig. 2, comprising the TP itself, the Himalaya, the Pamir, the Hindukush, the Tian Shan and the Southeast Asian highlands. In contrast, the Altai region in the northern part of our model domain was probably built prior to the TP uplift and, hence, is not modified (cf. Rowley and Currie, 2006; Wang et al., 2006). In fact, there is an ongoing debate about how to assess the regionally differentiated uplift process in the light of geological records (Liu and Dong, 2013; Liu et al., 2016). Some authors also argue that the Mongolian Plateau uplift may be younger than the rise of the TP (Windley and Allen, 1993). Given this uncertainty, we use a rather idealized uplift scenario without regionally differentiated uplift rates (cf. Tapponnier et al., 2001; Liu and Yin, 2002; Tang et al., 2013a; Zhang et al., 2014) nor a modification of the land-sea mask (cf. Fluteau et al., 1999) in order to facilitate the physical interpretation of the climate response to the stepwise uplift process. In order to avoid an artificial trough in Central Asia, a minimum height of 500 m above sea level is prescribed when reduced topography falls below this threshold. This is in agreement with Le Pichon et al. (1992) who suggested a base height of at least 500 m for the TP area prior to plateau uplift in the Cenozoic. Along the borders of the region with modified elevation, the discontinuous transition between modified and unmodified topography is smoothed by interpolation. As no spatially differentiated information on the land surface characteristics of the TP during the mid and late Cenozoic exists, vegetation cover and related surface parameters are kept constant at present-day level. This is justifiable in terms of an improved process understanding, but implies that the experimental setup is rather idealized and not necessarily indicative of the real paleo-climatic conditions in the late Miocene that, by the way, are barely inferable from available proxy data.

The resulting model topographies for the control run (100% elevation) and the 4 sensitivity studies with stepwise reduction of elevation are displayed in Fig. 2. It is obvious that for each simulation a continuous land surface without unnatural cracks and slopes is given. In addition, a part of the present-day relative topography across the TP region is retained. The control run with present-day elevation covers the period 1961–2000, the other time slices are also based on 40-year model periods. For validation and statistical analysis the first 10 model years are skipped in order to remove model spin-up effects during the first model years, as found in temperature and moisture of the deepest soil layer. The remaining 30 years ensure a climate equilibrium states of sufficient length for a thorough statistical assessment, including cluster analysis of present-day and paleo-climatic states.

The second type of REMO experiments pertains to the LGM and MH episodes. In this case, REMO is nested in a higher-resolution ECHAM5 version with T106 (~1.125°) and 31 vertical levels (Werner et al., 2011). This ECHAM5 version includes stable isotopes and has been analyzed in terms of $\delta^{18}O$ trajectories (Li et al., 2016, 2017) and governing factors of $\delta^{18}O$ (Mutz et al., 2016). The boundary conditions for the LGM and MH periods have been prescribed equally in ECHAM5 and REMO. This includes greenhouse gas concentrations, land surface characteristics, land-sea mask due to sea level changes (in ECHAM5), and orbital parameters (cf. Ruddiman, 2014). The specific boundary conditions for MH are described in detail by Dietrich et al. (2013). They are in agreement with the guidelines of the Paleoclimate Modelling Intercomparison Project Phase 3 (PMIP3, Arnold et al., 2009). Oceanic boundary conditions and sea ice coverage for present-day, LGM and MH are taken from a coupled ECHO-G model experiment (Lorenz and Lohmann, 2004). In REMO, the modified land cover classes are translated into monthly varying seasonal cycles of background surface albedo, fractional vegetation cover and leaf area index in order to account for the seasonal evolution of the Asian monsoon systems in a more appropriate way. Given the modified ECHAM5 resolution and model settings in ECHAM5 and REMO, an additional control run is realized covering the period 1978–1989. This period has been chosen because the long-term means of the meteorological variables required for the cluster analysis are very close to the respective long-term means during the 1961–2000 period considered for the uplift experiments. Thus, they represent virtually the same present-day climatology and results are not

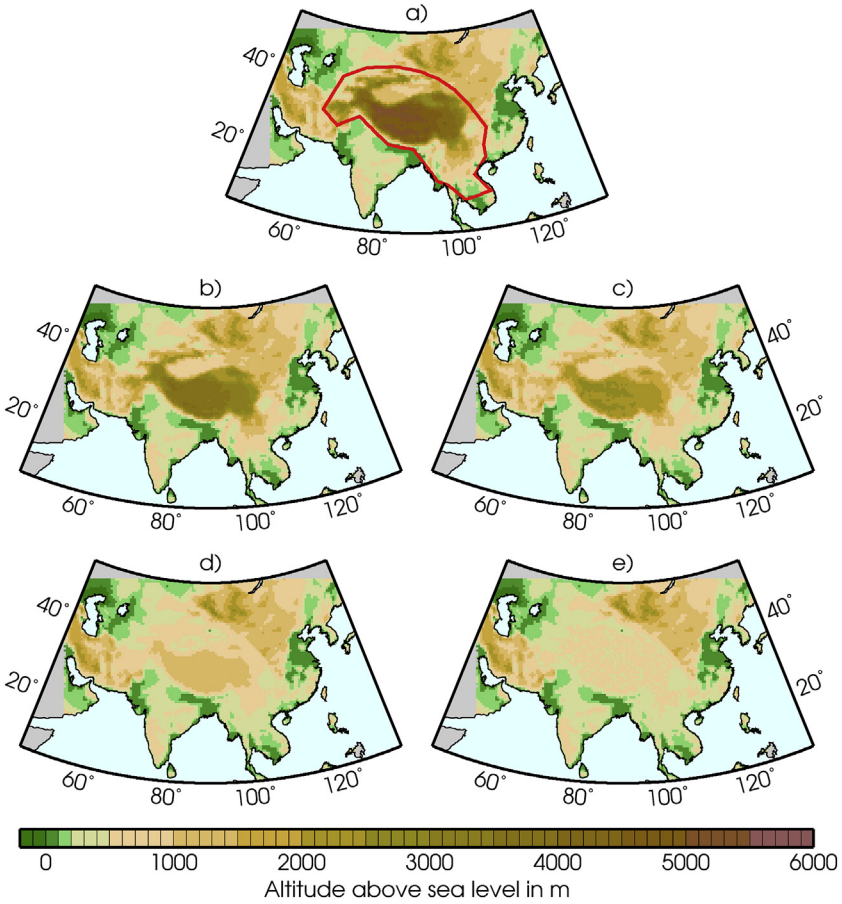

Fig. 2. Topography over Central Asia for the control run with present-day elevation (a) and the stepwise reduction to 75% (b), 50% (c), 25% (d) and complete leveling (e) compared with present-day elevation.

blurred by decadal-scale variations during the late 20th century. 12-year model periods are also applied to the LGM and MH episodes, retaining the last 10 years for model validation and statistical analysis of climate anomalies.

For the validation of the present-day climate simulated by ECHAM5 and REMO, we rely on several data sets (see Table 1 for resolution and time coverage): monthly temperature and precipitation data from the CRU data set, a gridded data product based on station observations over land (Mitchell and Jones, 2005), from the NCEP (Kalnay et al., 1996) and ERA40 (Uppala et al., 2005) reanalyses, and from the High Asia Reanalysis (HAR), a regional reanalysis with the RCM WRF at a resolution of 0.3° covering the period 2000–2012 (Maussion et al., 2014) which represents a benchmark for state-of-the-art high-resolution data sets for the TP region. Satellite-based precipitation products such as TRMM have not been considered due to distinct biases over the Himalaya and TP (cf. Barthi and Singh, 2015). The LGM and MH paleoclimatic episodes are compared with quantitative reconstructions of temperature and precipitation from mainly pollen-based proxy-data available over several 2° x 2° grid boxes across the TP and eastern Asia (Bartlein et al., 2011). This data set is also used as a reference for PMIP3 paleo-simulations. For a detailed description of the locations and underlying material of this compiled proxy-data set, refer to Li et al. (2017).

Table 1
Horizontal resolution and time coverage of the considered observational data sets.

Name	Resolution	Time coverage
CRU	0.5°	1901–2017
NCEP	1.9°	1948 to present
ERA40	2.5°	1958–2002
HAR	0.3°	2000–2012

The statistical significance of climate changes due to the uplift process and to the LGM and MH boundary conditions, respectively, is assessed by means of a one-way analysis of variance (Wilks, 2006), taking the offset of the means due to the changing boundary conditions as treatment effect and the year-to-year changes within the simulated time series as internal variability.

A special focus of our study is on the TP region and on the question if climate types have noticeably changed due to the various forcings. Therefore, a classification of the Tibetan climate is carried out by a hierarchical cluster analysis combined with a subsequent non-hierarchical k-means correction approach. This method is dedicated to achieve homogeneous clusters which are sharply distinguishable from each other (cf. Paeth et al., 2005; Wilks, 2006; Geng et al., 2014; Netzel and Stepinski, 2016). The cluster analysis is applied to the domain indicated by the rectangle in Fig. 1. It is based on seven equally weighted atmospheric variables, including annual-mean 2 m temperature, annual precipitation amount, annual temperature range, 10 m zonal and meridional wind components in January and July. In the first step, the hierarchical cluster analysis is used to determine an appropriate number of clusters and their multivariate centroids. It has been found that eight clusters provide the best result in terms of interpretable and discriminable climate types across the TP and surrounding regions. This means that the clusters are internally homogeneous and clearly differ from all other clusters. A larger number of clusters led to clusters of very small size in hilltop positions, a smaller number implied a loss of spatial differentiation on the TP itself. In the second step, the non-hierarchical k-means approach re-assigns all model grid boxes to the

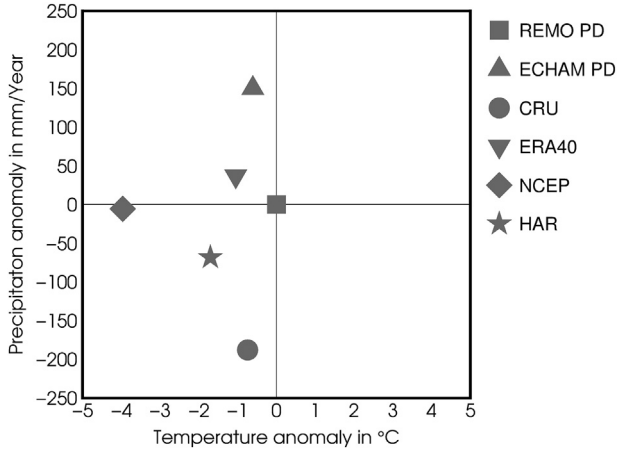

Fig. 3. Comparison of mean temperature and precipitation averaged over the cluster domain (cf. Fig. 1) and the time period 1971–2000 from the regional climate model REMO (PD = present-day), the driving global climate model ECHAM, the regional reanalysis HAR, the global reanalysis NCEP, and the CRU observational data set.

obtained eight multivariate centroids in order to overcome the problem of fixed classification with changing centroids in the hierarchical approach and to increase the overall robustness of the cluster analysis.

4. Results

4.1. Model validation

A comparison of annual temperature and precipitation averaged over the cluster domain (see Fig. 1) between REMO, ECHAM5 and various observational data sets is depicted in Fig. 3. The validation period is 1971–2000. The respective control run from REMO marks the origin of the graph and all other data sets are indicated as anomalies with respect to this control run. The considered gridded data set (CRU) and reanalyses (ERA40, NCEP, HAR) differ substantially. CRU is much drier in the TP region and NCEP noticeably cooler than ERA40 and HAR. The uncertainty on behalf of the observational data is at least as pronounced as the potential bias of the RCM REMO. In fact, REMO is quite close to the ERA40 reanalysis and the HAR data set. Note that the latter certainly represents a benchmark for present-day climate on the TP, but the available data period 2000–2012 is rather short and does not coincide with the simulation periods of ECHAM5 and REMO. The driving global climate model ECHAM5 is characterized by a strong wet bias on the TP. The spatial patterns of temperature and precipitation from REMO, ECHAM5 and the various observational data sets have a very similar structure (cf. Figs. 2 and 3 in Mannig et al., 2013). Yet, some noticeable discrepancies between all data sets occur over the high-mountain chains of Himalaya, Tien Shan, Pamir and Kunlun where temperature and precipitation differences amount to more than 4 °C and 500 mm per year, respectively (not shown). Discrepancies are much lower over the central parts of the TP where orographic variance is much smaller and climate data less sensitive to the horizontal resolution of the model or data set. Compared with ECHAM5, the bias is considerably reduced by dynamical downscaling and points to a clear added value of REMO compared with ECHAM5. This is consistent with the study by Mannig et al. (2013) who have validated REMO simulations driven by ERA40 reanalyses and ECHAM5/MPI-OM coupled climate model simulations over entire Asia and concluded that the RCM performs well over the continent and exhibits an added value with respect to the coarser-grid global climate model. Thus, our second scientific hypothesis can be corroborated, at least in terms of present-day climate.

A more detailed validation of REMO in the model domain and version presented here has been conducted in the framework of another paper in preparation. It demonstrates that REMO is able to reproduce the observed main characteristics of climate on the TP and in surrounding regions. Especially temperatures at high-elevation sites are well captured and clusters of distinct climate types agree almost perfectly between REMO, ERA40 and HAR. Therefore, it is assumed that REMO provides a reliable basis to simulate paleo-climatic changes.

4.2. Surface uplift experiments

The temperature changes associated with the surface uplift of the TP and surrounding mountain areas are illustrated in Fig. 4. As the plateau itself and the Asian monsoon systems are subject to a distinct seasonal regime, results are shown for annual means, winter means (DJF) and summer means (JJA). Indeed, the annual temperature range increases from south to north and amounts to more than 40 °C between winter and summer in Central Asia and in parts of the TP (Fig. 4, top panels). It is also obvious that near-surface temperature is a stringent function of elevation. Thus, reduced elevation leads to higher temperature over the TP, simply due to the thermal stratification of the atmosphere (Fig. 4, panels d–o). The warming amounts to more than 30 °C in the experiment with 0% of present-day elevation (with a minimum height of 500 m on the TP). The warming increases more or less linearly with reduced topography. On the TP itself, warming rates in winter and summer are virtually the same. Central Asia is marked by a slight cooling and the continental desert region north of the TP by a noticeable cooling in both seasons, amounting to more than 7 °C, especially in winter. Later on, this will be explained by changes in precipitation and large-scale mid-latitude circulation. Over South Asia, reduced elevation implies lower temperature in winter and slightly warmer conditions in summer. While the first effect is probably associated with an enhanced intrusion of cold air masses from the continent due to the missing barrier of the Himalaya and TP, the latter effect is linked to reduced precipitation amount (see below). Thanks to the high resolution of REMO, the resulting climate change patterns are characterized by numerous regional details such as the basin structure on the northeastern TP, the fine-scale changes in the Tian Shan mountain range and the desert basins in western China.

Fig. 5 displays the respective annual-mean climatology of temperature from the global climate model ECHAM5 (top left panel). While the basic structure is virtually identical, some important regional features like the entire Tian Shan mountain range and the differentiated topography of the TP itself are not at all resolved by the large-scale model. Compared with REMO, ECHAM5 also underestimates the regional heterogeneity of the temperature pattern across Central Asia. The experiment with 0% topography leads to a similar but spatially less coherent temperature signal in ECHAM5 with respect to REMO, e.g. over India and on the Mongolian Plateau (Fig. 5, panel c). There are also qualitative differences in the temperature response, especially in the Tarim basin and downstream the Tian Shan mountain chain because the barrier effect of the latter is not accounted for by the low-resolution ECHAM5 model. In the light of missing high-resolution proxy-data for this distant paleo-climatic episode, it is of course difficult to judge whether these differences between REMO and ECHAM5 can be interpreted as an added value of dynamical downscaling on the basis of sensitivity studies. Yet, for the climatological patterns this added value is quite obvious (see Subsection 4.1).

The impact of the stepwise uplift on annual, winter and summer precipitation is portrayed in Fig. 6. In the South and East Asian monsoon regions precipitation is mainly a summer phenomenon, whereas the mid-latitudes in Asia follow a more equalized seasonal regime (Fig. 6, top panels). The precipitation response to reduced elevation is marked by a spatially heterogeneous picture (Fig. 6, panels d–o). The TP, South Asia, eastern China and the southern part of Central Asia exhibit drier conditions. In the monsoon areas this amounts to less than 50%. In Central Asia the relative drying is more important. However,

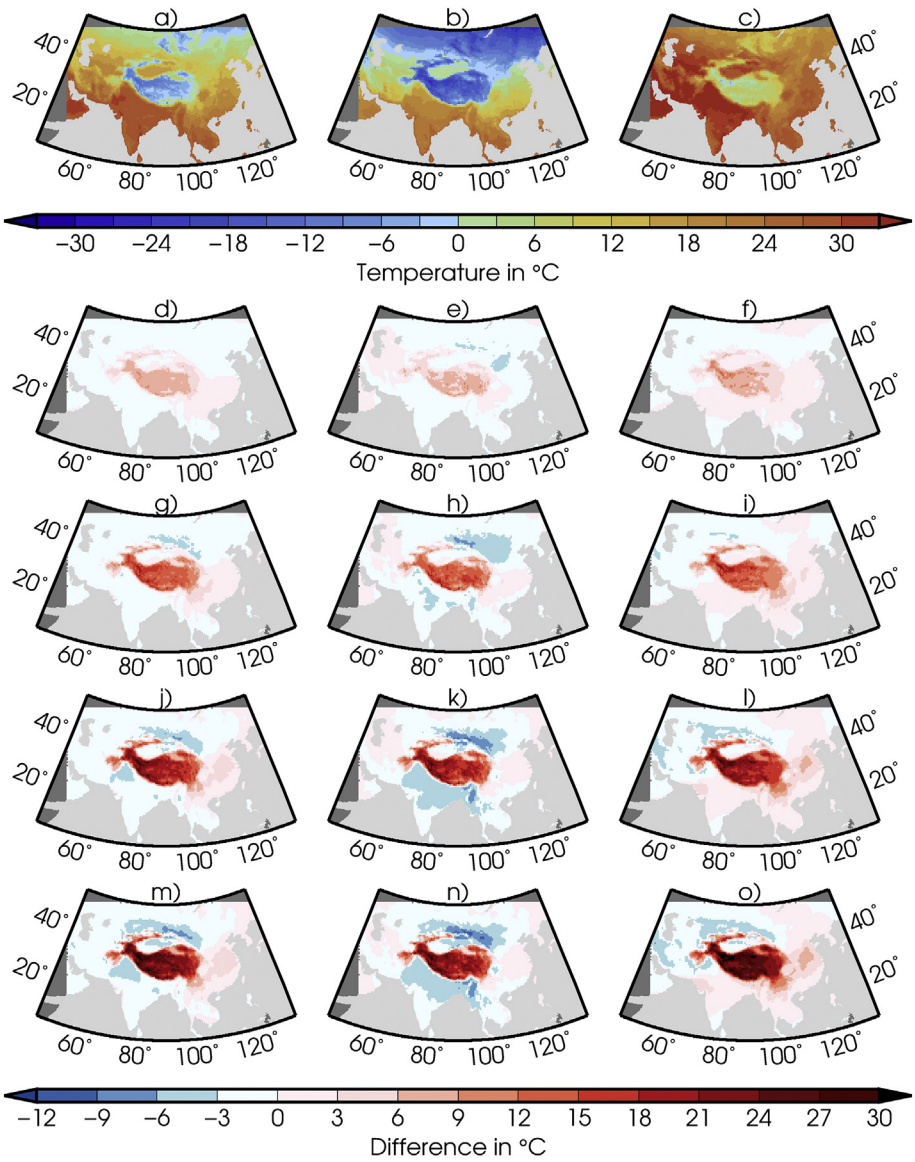

Fig. 4. Near-surface temperature averaged over the control period 1971–2000 (top row) for annual means (left column), winter means (middle column) and summer means (right column) as well as temperature changes (sensitivity experiment minus control) due to a stepwise reduction of elevation (d-o) from T075 (upper panels) to T000 (lower panels).

the most striking feature in the precipitation response is simulated over the continental arid regions of western China and northwestern Central Asia. Indeed, precipitation increases by up to 250%, when the plateau height is reduced to 25%. This rises to up to four times more than the present-day climatology in some arid regions and is related to circulation changes and related moisture advection (see below). As for temperature, the major changes occur up to a reduction to 25% of present-day elevation, while the 0% experiment only increases the precipitation on the TP itself. An interesting regional detail is given by the wetter conditions in winter along southeastern and eastern India and Southeast Asia. For India, this can be explained by the missing barrier effect of the eastern Himalaya and TP that leads to a reduced adiabatic warming at its southern slope from the perspective of the northeasterly winter monsoon and downstream more relief rainfall along the Garo-Khasi range and the Eastern Ghats in India that also receive some winter rainfall under present-day conditions. For Southeast Asia where topography is unchanged and the impact of the TP much less important, the precipitation increase cannot be explained easily. In fact, this increase is very small in absolute numbers given winter precipitation sums below 20 mm under current climate conditions. Again, the global climate model ECHAM5 misses some important regional details of the precipitation climatology (Fig. 5, top right) and the precipitation changes due to reduced elevation barely account for any spatial differentiation across the TP, in the Taklamakan desert and in eastern China (Fig. 5, panel d).

To assess the importance and statistical significance of temperature and precipitation changes due to the uplift process, a one-way analysis of variance has been applied using pairs of uplift experiments or all uplift experiments at once. The analysis of variance reveals that the stepwise uplift scenario accounts for more than 90% of total annual temperature variability on the TP (Fig. 7, top panels). This implies that the topographic forcing between the 30-year time slices dominates by far the internal year-to-year fluctuations of temperature within the time slices. This effect is already achieved in the 75% experiment. In the surrounding regions, the uplift effect is less pronounced, ranging between 20% and 80% of explained variance. Nevertheless, the temperature changes are statistically significant in almost the entire model domain. For precipitation the picture is more dispersed (Fig. 7, bottom

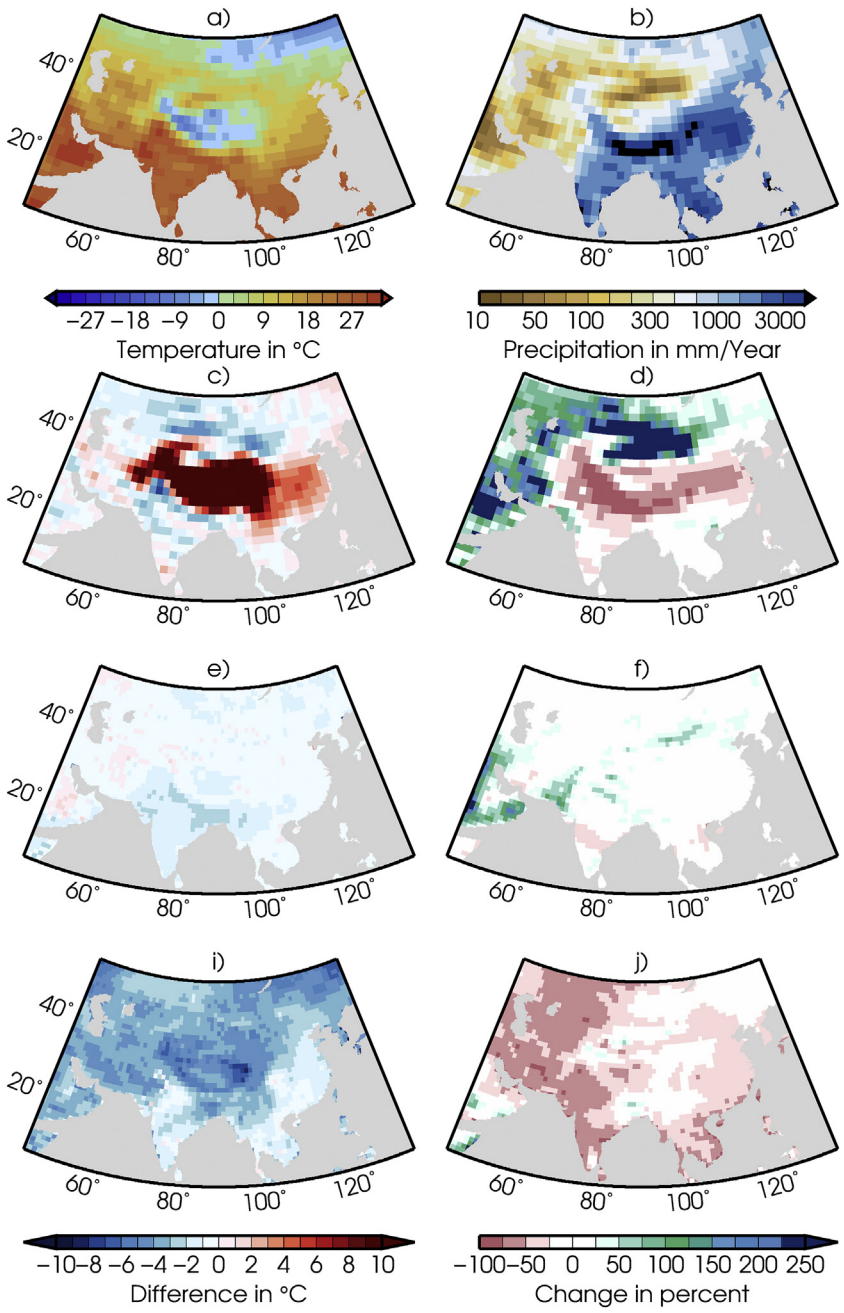

Fig. 5. Annual near-surface temperature (left column) and total precipitation (right column) from the global climate model ECHAM averaged over the control period 1971–2000 (top row) as well as changes (sensitivity experiment minus control) due to a reduction of elevation to T000 (second row), MH forcing (third row), and LGM forcing (bottom row).

panels) and the uplift effect is much less pronounced in the 75% experiment: Precipitation is characterized by substantially stronger internal variability than temperature (e.g. IPCC, 2013) and, hence, the uplift process accounts for a smaller portion of total variance. Nonetheless, the explained variance reaches up to 90% in the arid regions of western China, where the uplift comes along with a multiplication of present-day precipitation amount.

In the following, the substantial drying of the desert basins of western and northern China during the uplift phase is analyzed in more detail. At first sight, this may be interpreted as an increasing barrier effect of the topography, hindering the moist summer monsoon flow from the northern Indian Ocean to penetrate far into the Asian continent. However, a deeper look on the wind components in various atmospheric levels before and after the uplift reveals that in none of the uplift experiments the monsoon air masses propagate into the arid regions of western China, rather these are characterized by extratropical westerlies independent of the topography (not shown). The clue to the problem is given by changes in the extratropical wave train and associated moisture advection processes. Fig. 8 displays the mean position of troughs and ridges in the 500 hPa geopotential height field under present-day conditions (top panel) and the respective changes in the 50% and 0% experiments (bottom panels). Mid-tropospheric geopotential height governs the geostrophic wind that represents the prevailing component of large-scale atmospheric circulation at this level (cf. Paeth et al., 2015). Under present-day conditions, long-term mean geopotential height is higher over Central Asia and lower over northeastern Asia, indicating the typical position of ridges and troughs, respectively, in the extratropical Rossby waves. The climatological

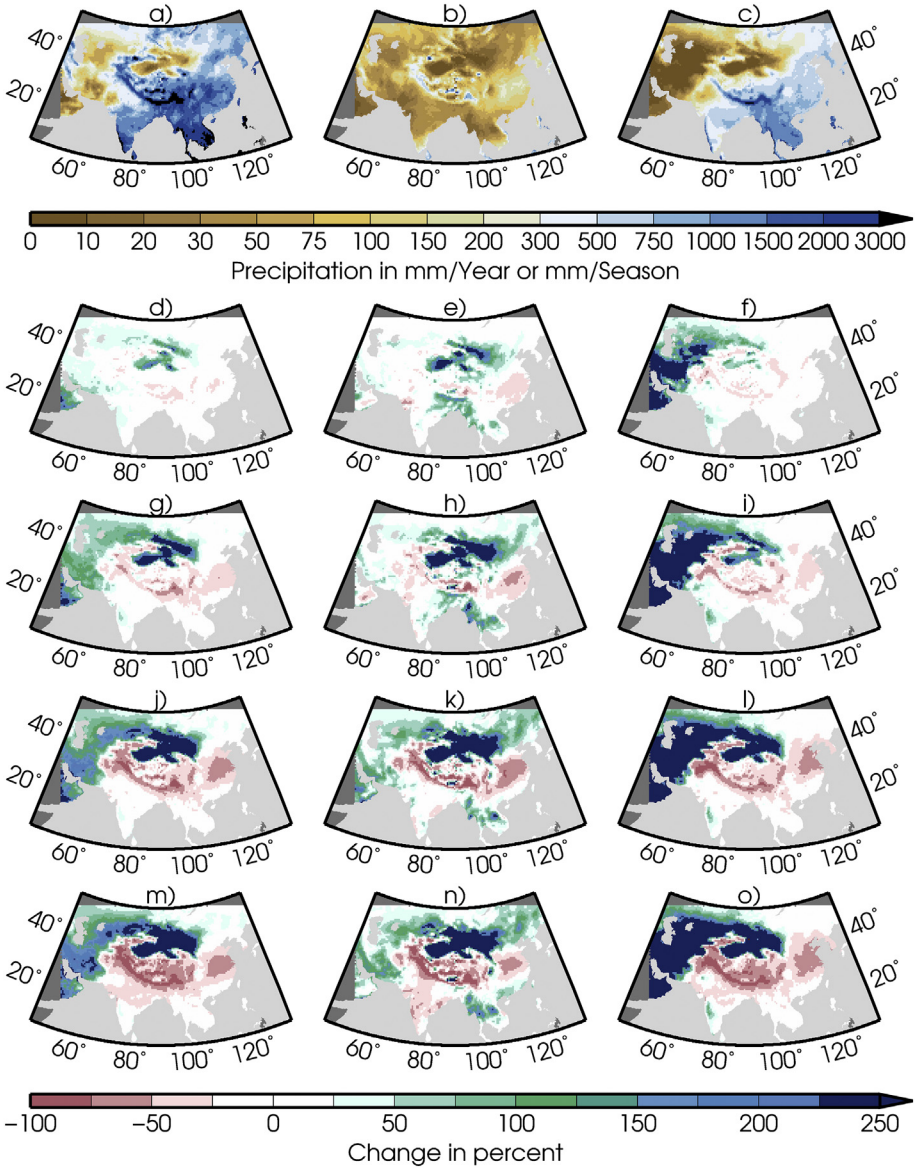

Fig. 6. Same as Fig. 4 but for total precipitation.

pattern in Fig. 8a represents the well-known Northern Hemisphere zonal wave number 3 structure with southwesterly flow on average over western Asia and northwesterly flow over eastern Asia. Under the quasi-stationary high-pressure ridge over Central Asia and north of the TP precipitation is largely suppressed under current climate conditions, leading to desert-type and arid climate characteristics. Reduced elevation of the TP implies a substantial large-scale decrease of geopotential height over Central Asia. This appears to be the key mechanism of how the uplift process in the TP regions affects extratropical climate all around the globe (cf. Molnar, 2005): the reduced barrier effect of the TP and adjacent mountain chains leads to a westward shift of the stationary wave train and induces cyclonic anomalies, enhanced static instability and atmospheric uplift over Central Asia. At the forefront of the trough that is located exactly over the region where the precipitation increase peaks in northwestern China, southwesterly flow with enhanced moisture advection prevails (cf. Hahn and Manabe, 1975).

The last aspect addressed from the uplift experiments pertains to the identification of distinct climate types on the TP and adjacent regions and their sensitivity to the uplift process. In the high-dimensional climate system, climate types often allow for a more comprehensive interpretation of climate changes than individual grid boxes (e.g. Paeth et al., 2005; Geng et al., 2014; Netzel and Stepinski, 2016). Fig. 9 presents a climate classification based on eight clusters derived from the 30-year REMO control run (top panel). The clusters are arranged from warm climates (red) to cold climates (blue). The remaining panels refer to the experiments with reduced elevation, but use the cluster centroids from the control run. Under present-day conditions, the desert Thar in western India occupies cluster 1 which is characterized by very high temperature and low annual rainfall amount. Northwestern India is marked by cluster 2 with still rather high temperature but more humid conditions. Cluster 3 represents the southern slopes of the Himalaya where climate is cooler but annual precipitation exceeds 3000 mm/yr. Cluster 4 is characterized by intermediate temperature and very dry conditions and covers the continental deserts with less than 100 mm of annual precipitation, particularly in the Tarim basin. Cluster 5 extends along the foothills on the northern side of the TP, the Tian Shan and the Pamir as well as over the less arid regions of western China. It denotes a colder and more humid climate than cluster 4. The southern and eastern part of the TP is given by cluster 6. Annual mean temperature is below 0 °C and rainfall exceeds 1500 mm per year. This cluster denotes those parts of the TP on the wind-ward side that are more influenced by moist air advection from the South Asian summer

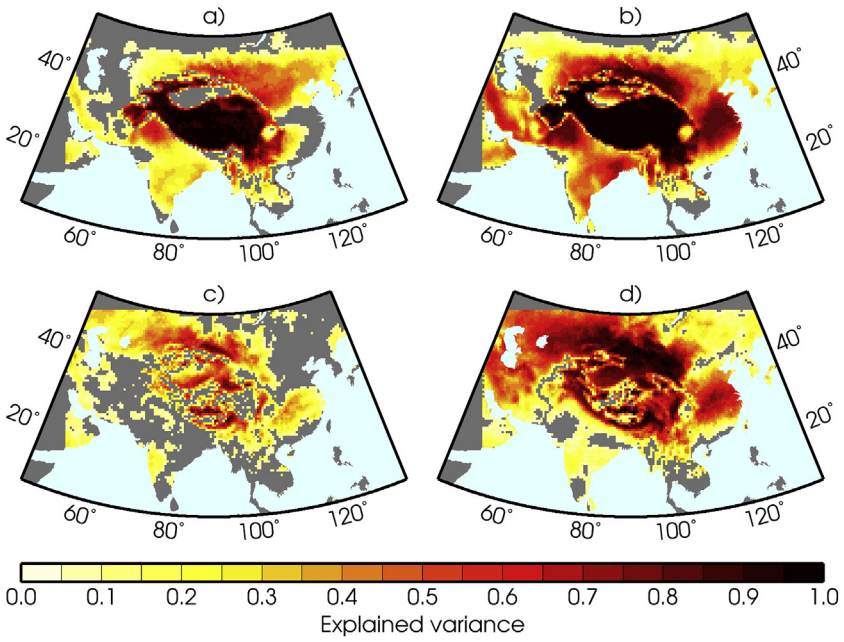

Fig. 7. Portion of variance explained by the uplift of the Tibetan Plateau as inferred from a one-way analysis of variance for near-surface temperature (top panels) and total precipitation (bottom panels) assessed between the T100 and T075 experiments (left column) and between all uplift experiments T100 – T000 (right column). Only values significant at the 5% level are plotted.

monsoon. In contrast, cluster 8 stands for the much drier and even colder northern part of the TP. Cluster 7 is rather peculiar: it spreads over those areas of the plateau that are marked by a large number of lakes. In the vicinity of these lakes, REMO simulates a climate that is as cold as the one in cluster 8 but with precipitation totals of up to 2000 mm/year. Later on, this cluster will be identified as a model artefact.

The experiments with reduced topography manifest a stepwise shift of these climate types towards a setting where the TP exhibits a much warmer and drier climate (Fig. 9, panels b–e). North of the TP, climate switches from the continental desert type to a much colder and more humid type which is confined today to the northern foothills of the TP. Altogether, the climate classification of the 0% experiment leads to a pattern which fundamentally differs from the one under present-day conditions, highlighting the tremendous impact of the uplift process on climate types on and around the TP.

4.3. Mid-Holocene and LGM experiments

The simulated temperature anomalies during the LGM and MH episodes are illustrated in Fig. 10. Again, it is differentiated between annual, winter and summer means. Note that the control run for these time slices is slightly different from the one for the uplift experiment and only 10 years per run are available for analysis because the

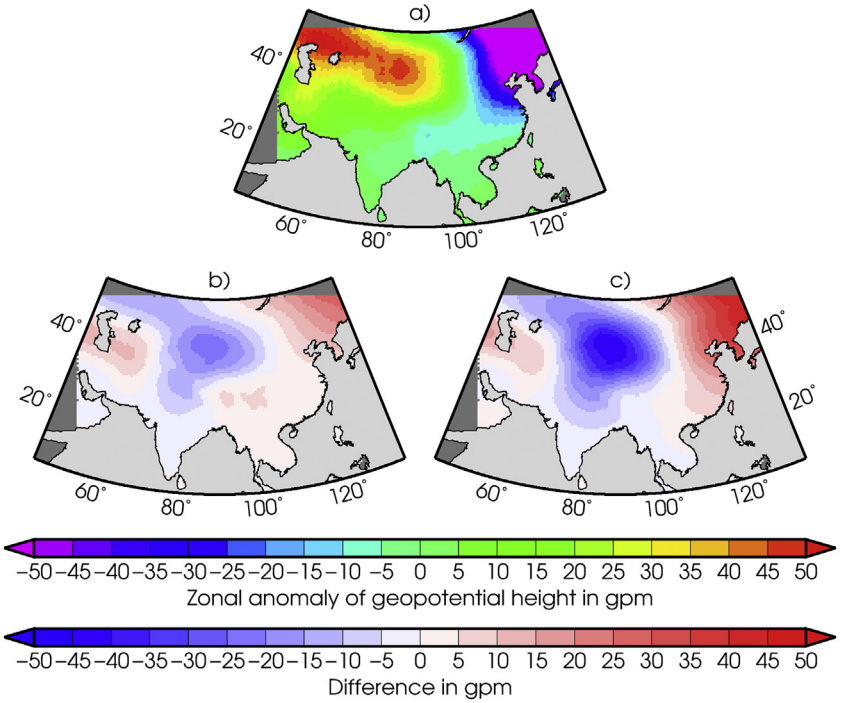

Fig. 8. Anomalies of annual-mean 500 hPa geopotential height from the zonal mean averaged over the control period 1971–2000 (a) and changes due to a stepwise reduction of elevation in the T050 (b) and T000 (c) experiments.

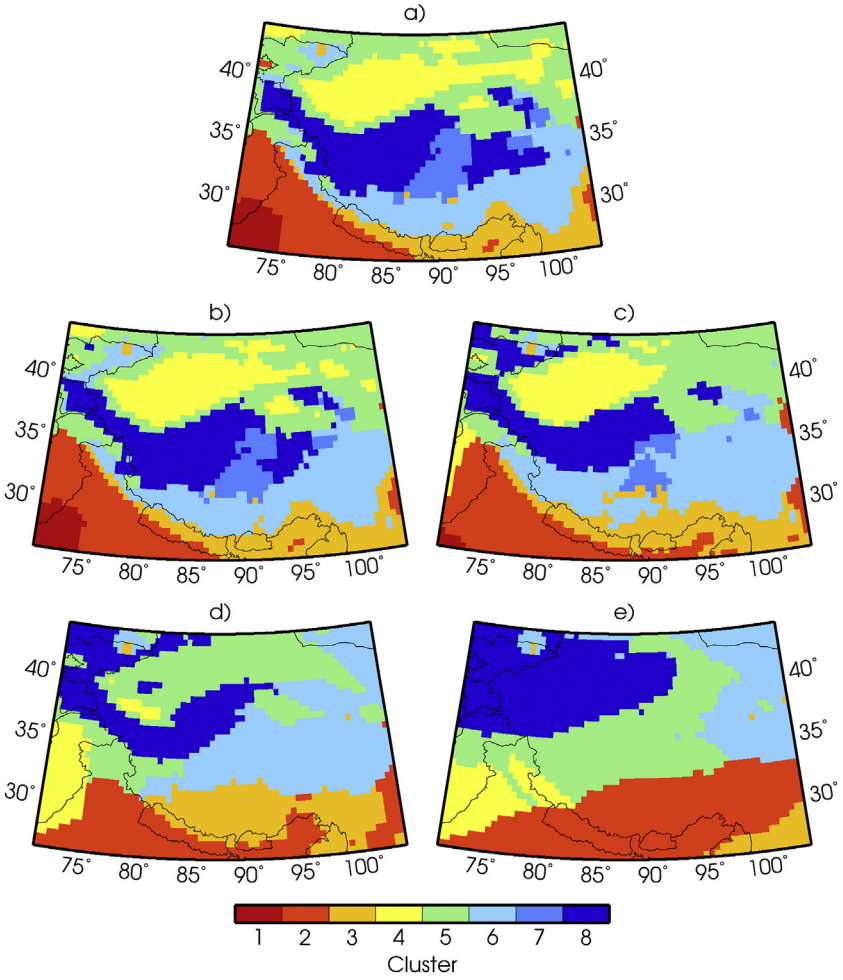

Fig. 9. Results of the cluster analysis prescribing 8 clusters in the Tibetan Plateau region for the control period 1971–2000 (a) and projection of the uplift experiments T075 (b) to T000 (e) onto the same centroids from the control period. The numbering of the clusters is arbitrary.

ECHAM5 simulations used for the lateral boundary conditions have much higher resolution and, thus, have been computationally more expensive. It is obvious that the temperature response during the LGM period is much more pronounced than during the MH time slice. The LGM exhibits lower temperatures in virtually the entire model domain. The cooling amounts to 3–8 °C with largest amplitude on the TP. During the MH, the picture is more heterogeneous and temperature changes do not exceed 3 °C. Most regions undergo slightly colder conditions, except for the extratropical part of Asia in summer. The cooling effect peaks over the TP and, in particular, along the southern foothills of the Himalaya. Compared with REMO, the ECHAM5 model simulates a similar but spatially less heterogeneous temperature response and the cooling is slightly more prevailing across the entire model domain during both episodes, MH and LGM (Fig. 5, panels e + i).

The precipitation response during the LGM and MH periods is spatially rather incoherent (Fig. 11). During the LGM, drier conditions prevail in most parts of Asia, especially in Central Asia and the Middle East. Higher-elevation sites with southward exposition along the Himalaya, the Pamir, the Tian Shan and the Altai may have experienced more precipitation. The most striking feature, however, is the rainfall increase in winter by more than 100% over eastern India, Bangladesh and parts of Southeast Asia. In total numbers, this increase is less impressive since the present-day winter totals are in the order of 10 to 50 mm (cf. Fig. 6b). We have no reasonable physical explanation for such a process and assume it to be a model artefact because this precipitation signal does not show up in the driving ECHAM5 model nor can be corroborated by available proxy data (see below). From other study regions, we know that precipitation in REMO is quite sensitive to changes in vegetation cover, especially forest fraction (Paeth et al., 2009), and to tropical sea surface temperatures (Paeth et al., 2005). Therefore, it is suggested that the precipitation increase arises from deficiencies in or a wrong model response to the prescribed LGM land cover characteristics or Bay of Bengal oceanic boundary conditions in Northern Hemisphere winter.

The MH episode appears to be subject to slightly more annual precipitation amount in most parts of the model domain, except for Central India and the Middle East. This increase mainly takes place during the summer season, probably initiated by a stronger monsoon flow in East Asia and more advection of moist air masses by westerlies in the extratropics. The pattern of summer precipitation changes is consistent with the temperature response in Fig. 10: higher temperatures north of the TP provoke a northward shift of the summer monsoon flow with more rainfall along the Himalaya and the TP. Vice versa, higher rainfall in northern India and over the foothills of the Himalaya implies a cooling in these areas. The amplitude of precipitation changes due to MH and LGM conditions is reduced and much more homogeneous in space in ECHAM5 compared with REMO (Fig. 5, panels f + j). During MH, the precipitation signal almost disappears, while a rather homogeneous drying prevails during the LGM episode.

The analysis of variance demonstrates that the impact of LGM and MH boundary conditions on temperature and precipitation does not everywhere stand out from internal variability (Fig. 12). During the LGM period, the effect on near-surface temperature is outstanding with more than 90% of explained variance, especially on the TP, in Central

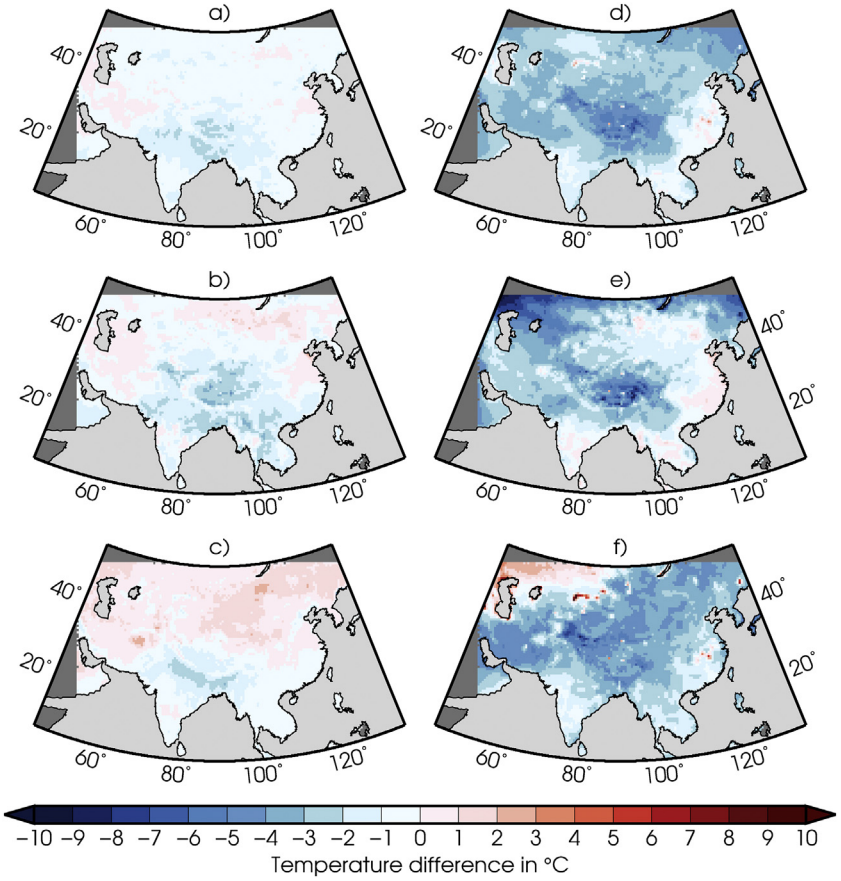

Fig. 10. Changes (sensitivity experiment minus control) in near-surface temperature for annual means (top row), winter means (middle row) and summer means (bottom row) as simulated by the MH (left column) and LGM (right column) experiment compared with the 1980–1989 control period.

Asia and the Middle East. In contrast, the MH episode produces a weaker temperature response, which peaks over South and Southeastern Asia. Only a part of the TP region is significantly affected by the MH boundary conditions. Typically, the forcing accounts for 20% to 70% of total temperature variance. For precipitation, the picture is even more dispersed: the MH is barely characterized by a coherent rainfall response pattern and, thus, the changes denoted in Fig. 11 should not be over-interpreted, except for the wetter conditions in the southern and western part of the TP. The LGM only leaves a mark in western and southeastern Asia where precipitation is below present-day totals. However, the explained variance ranges mostly below 50%.

In Fig. 13 the simulated annual temperature and precipitation changes during the LGM and MH episodes are compared with available quantitative reconstructions from pollen-based proxy-data (Bartlein et al., 2011). Note that in contrast to Fig. 11 the precipitation response is expressed in mm per year and not in percentage. The MH period is much better represented by proxy-data than the LGM (cf. Clift and Plumb, 2008; Bartlein et al., 2011). During the LGM episode, there is a good agreement between simulated and reconstructed temperature and precipitation, although this comparison is based on a small number of grid boxes (Fig. 13, right panels). Colder and drier conditions over China and Central Asia are likewise suggested by REMO and proxy-data. The two neighboring reconstructed pixels over the western Tian Shan with opposite temperature changes obviously reflect a data artefact. The simulated phenomenon of substantial rainfall increase north of the Bay of Bengal (see Fig. 11c) cannot be evaluated by means of proxy-data by reason that they are not available in this region. Anyway, we do not expect that proxy data, if available, would give support to this model feature but rather judge it as a model artefact.

During the MH, the pattern is more complex (Fig. 13, left panels): reconstructions indicate a small-scale coexistence of warmer and colder conditions over the TP, China and Central Asia, whereas in REMO a slight cooling prevails over most of the model domain. On the part of the reconstructions, the temperature response varies by up to 10 °C, partly with opposite sign, over a distance of some hundreds of kilometers. This reflects a large amount of uncertainty in the proxy-data, while the RCM produces a spatially coherent response pattern. In terms of precipitation, there is a satisfactory agreement between model and reconstructions: wetter conditions prevail over the TP, China and parts of Central Asia.

Finally, Fig. 14 clearly reveals that the spatial distribution of main climate types over the TP and surrounding regions is more or less insensitive to the modified boundary conditions during the LGM and MH periods. Note that in this case the reference clusters for present-day climate have been derived from a shorter period and, hence, the present-day pattern differs slightly from the one in Fig. 9 in terms of clusters 6 and 7, although the underlying long-term means are quite close to each other. Under LGM and MH conditions the climate classification barely changes. This is surprising given the simulated temperature and precipitation changes presented in Figs. 10 and 11, especially with respect to the considerably colder conditions during LGM. However, the cluster analysis is based on seven atmospheric variables that have equal weights when assigning grid boxes to cluster centroids (see Section 3). Thus, when temperature changes noticeably but the clusters remain stationary, this is a clear indication that the other atmospheric variables in the cluster analysis – i.e. wind components, annual temperature range and seasonal precipitation – cannot be substantially affected by the modified boundary conditions during LGM and MH. This is a major difference from the uplift experiments (see Fig. 9) and a clear objection to our first underlying hypothesis saying

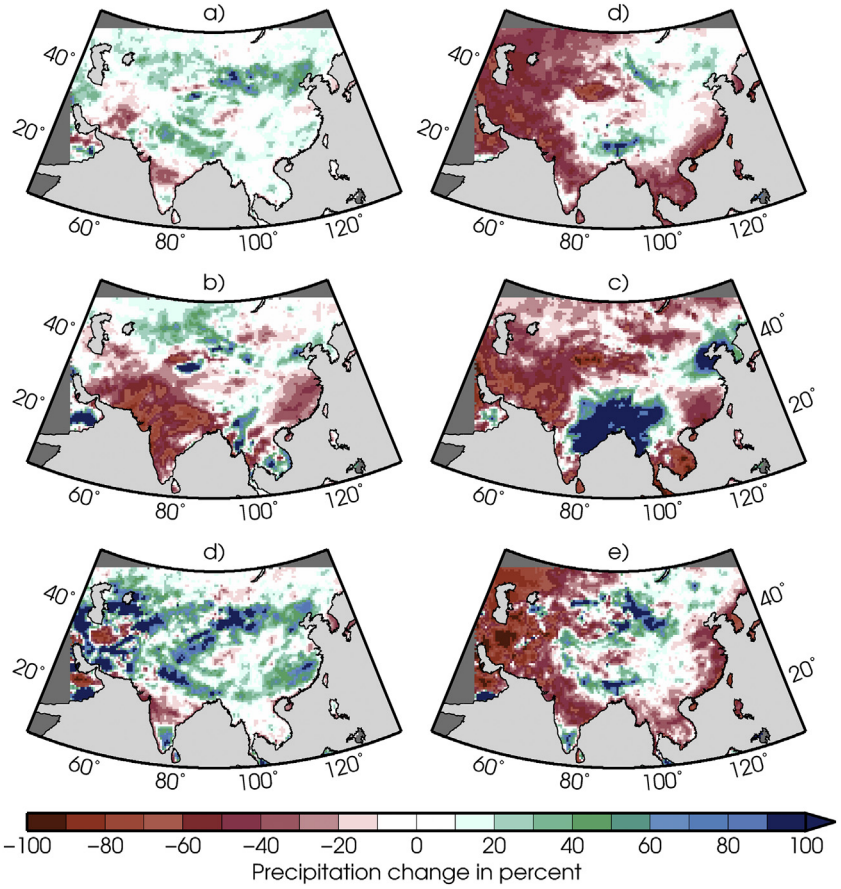

Fig. 11. Same as Fig. 10 but for total precipitation.

that orbital forcing can produce climate variations in the TP region that are comparable to the Cenozoic uplift phase.

4.4. Comparison of episodes

In the last step of our analysis the annual temperature and precipitation changes under uplift, LGM and MH conditions are directly compared with each other, once as regional means over the entire

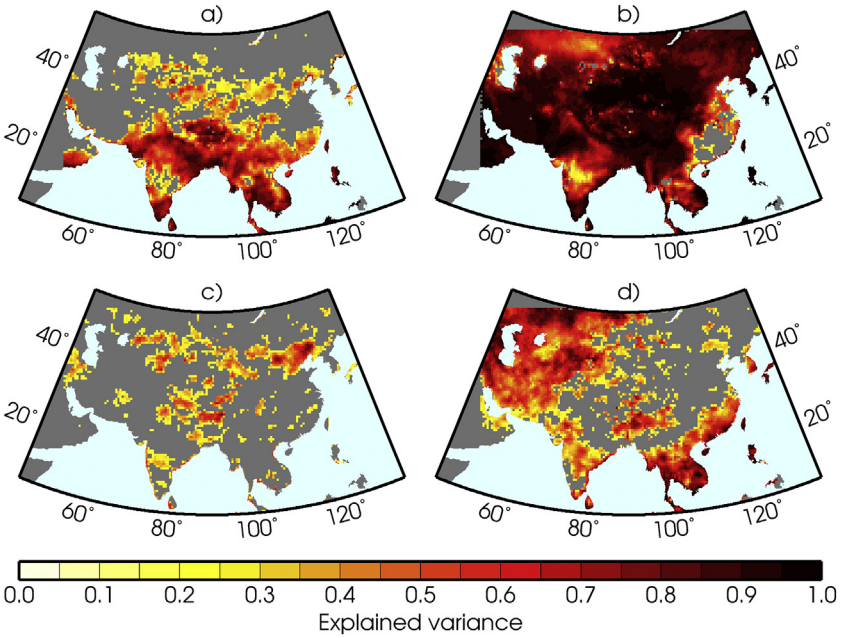

Fig. 12. Portion of variance explained by the MH (left column) and LGM (right column) experiment as inferred from a one-way analysis of variance for near-surface temperature (top panels) and total precipitation (bottom panels). Only values significant at the 5% level are plotted.

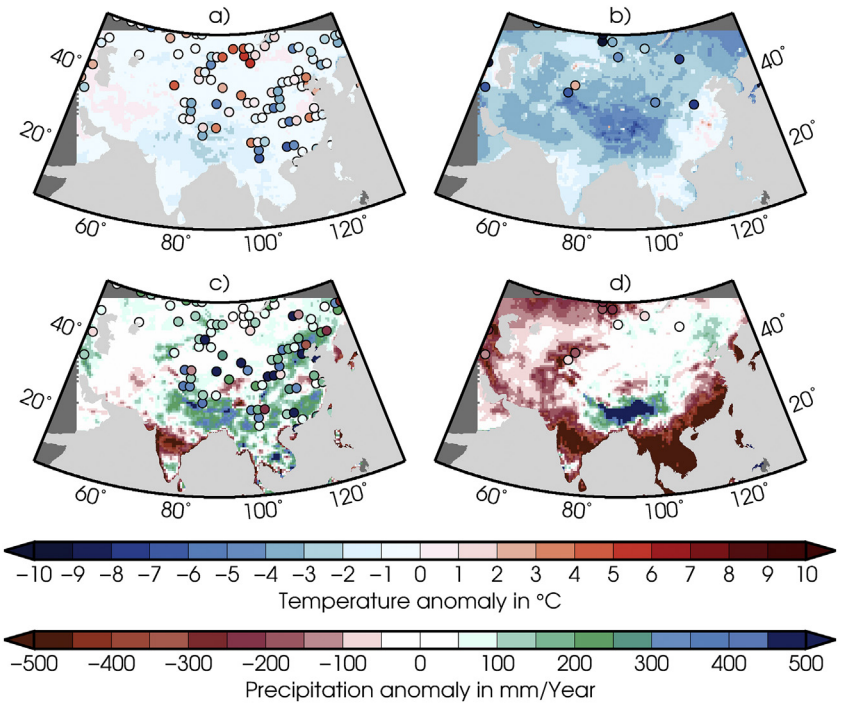

Fig. 13. Comparison of simulated mean annual temperature (top row) and total precipitation (bottom row) changes (sensitivity experiment minus control) in the MH (left column) and LGM (right column) period with available paleo-climatic reconstructions (filled circles) from proxy data based on pollen analysis (Bartlein et al., 2011).

cluster domain and once as averages over each individual cluster (Fig. 15). In addition, the results from REMO and ECHAM5 are compared with each other in order to assess which model type is associated with a higher sensitivity. Over the cluster domain, the strongest temperature and precipitation response is found for the uplift experiments, denoting a noticeably drier and warmer climate on and around the TP (top left panel). There is an offset between ECHAM5 and REMO (cf. Fig. 3) but the response is very similar. In both models, the largest changes occur between the 100%, 75% and 50% experiments, whereas the uplift from 0% to the 25% simulation plays a minor role. The LGM and MH affect the mean climate in the cluster domain to a much lower extent. The response in REMO and ECHAM5 is again similar, with one exception: REMO simulates slightly wetter conditions, mainly due to the outstanding precipitation increase over the southeastern TP (see Fig. 11), while ECHAM5 suggests a drying.

Fig. 15 also indicates that the striking climate changes during the uplift process are mainly performed by clusters 3, 6, 7 and 8. These clusters represent the higher-elevation sites and southward slopes of the TP and Himalaya, respectively. The changes in cluster 3 and 8 even lie outside the illustrated precipitation and temperature range, respectively, highlighting the enormous drying along the southern slope and warming on the northern TP at reduced elevation. In addition, clusters

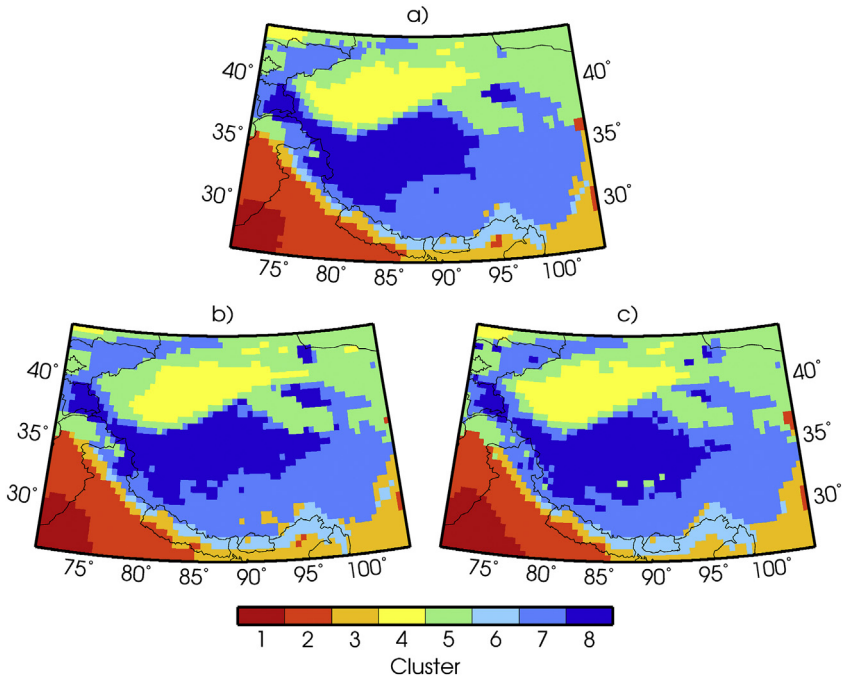

Fig. 14. Results of the cluster analysis prescribing 8 clusters in the Tibetan Plateau region for the control period 1980–1989 (a) and projection of the MH (b) and LGM (c) experiments onto the same centroids from the control period. The numbering of the clusters is arbitrary.

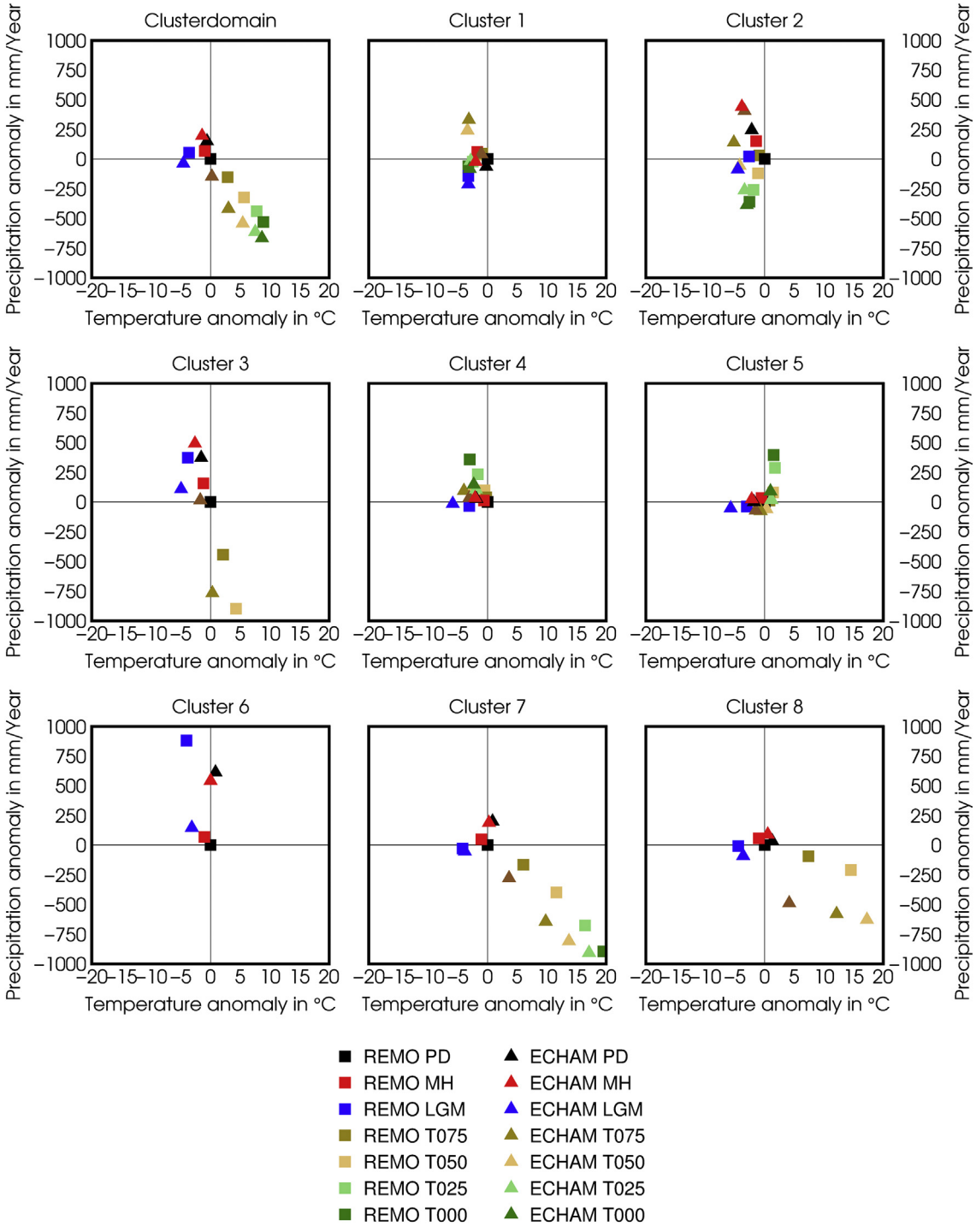

Fig. 15. Synthesis of changes in annual mean near-surface temperature (x-axis) and total precipitation (y-axis) averaged over the entire cluster domain (top left) and over the individual 8 cluster regions (remaining panels) from the uplift, MH and LGM experiments compared with the respective control periods, once for the regional climate model REMO and once for the driving global climate model ECHAM.

4 and 5 experience a substantial precipitation increase in the 25% and 0% experiments, suggesting that the continental dry climate north of the TP did not exist during the early uplift phase (cf. Fig. 6). This effect is only simulated by REMO at higher spatial resolution. LGM and MH have mainly affected the clusters 3, 4, 5 and 6. Clusters 4 and 5 are representative of the arid and semi-arid climate types north of the TP. Nonetheless, temperature over the TP (clusters 7 and 8) also decreases considerably under LGM conditions. In most cluster regions around the TP, the climate changes during LGM and MH are of the same order of magnitude as during the uplift process. In contrast, the TP itself is much more sensitive to the plateau uplift and, hence, stronger signals should be expected in proxy-data for that earlier period.

5. Discussion

This study provides new insight into prominent Cenozoic and Quaternary paleo-climatic variations in Asia and, more specifically, in the TP region. Several novel aspects have been addressed: (1) the use of a high-resolution regional climate model and the comparison with its driving global climate model, (2) the realization of long-term

equilibrium state experiments that allow for a more sophisticated statistical assessment including cluster analysis and analysis of variance, and (3) the quantification and comparison of natural climate variations arising from orbital forcing and surface uplift within a consistent modeling framework.

The comparative validation of the RCM REMO and the driving global climate model ECHAM5 has shown that the higher-resolution model provides temperature and precipitation patterns with much more regional details in this orographically shaped area and is closer to the available observational data and reanalyses, particularly with respect to precipitation. This is consistent with other studies highlighting the added value of higher-resolution climate models in Asia and other regions of the globe (e.g. Kitoh et al., 2010; Paeth et al., 2011; Mannig et al., 2013; Paeth et al., 2015; Paxian et al., 2015).

The uplift experiments with stepwise reduction of topography describe a continuous transition towards a warmer and drier climate on the TP when elevation decreases. This general tendency has been found in virtually all uplift experiments since the pioneering work by Hahn and Manabe (1975) and Kutzbach et al. (1989, 1993). Another earlier finding, which we could corroborate with this study, is the fact that the later uplift process has played a more important role for the TP climate and surrounding monsoon systems than the early phase. In our study, the changes are stronger between the 100%, 75% and 50% experiments than between the 25% and 0% simulations. Kitoh et al. (2010) have reported that their 60% experiment represented a threshold for accelerated climate change. A novel aspect of our modeling design pertains to the high spatial resolution and, at the same time, the relatively long simulation periods for the time slices, which allow for a more sophisticated statistical assessment of changes and their significance. Another important finding arising from the high resolution of the REMO model concerns the appearance of the continental-desert type of climate that first occurred in the transition from the 25% to the 50% experiment (cf. Liu et al., 2015). This process is probably related to dynamical changes in the extratropical Rossby wave configuration. The identification of climate types by means of cluster analysis has proven to be an instructive tool to illustrate multivariate changes at the scale of regional climates (cf. Geng et al., 2014; Netzel and Stepinski, 2016). In fact, it could be shown that the uplift process induces a fundamental rearrangement of present-day climate types on the TP and in surrounding regions, especially to the north (cf. Liu et al., 2015).

During the LGM period, REMO simulates colder conditions in most regions of Asia with the largest temperature decrease in winter over the TP and in the northernmost part of the model domain along 60°N. This is in agreement with previous modeling studies (e.g. Liu et al., 2008a, 2008b; Harrison et al., 2014) and reconstructions (e.g. Mischke et al., 2013; Saraswat et al., 2013). The cooling in our model ranges between 3 °C and 8 °C on the TP, which agrees well with proxy-data from Bartlein et al. (2011). In contrast, other authors have stated that the LGM cooling rate is underestimated by their global (Harrison et al., 2014) and regional (Zheng et al., 2004; Ju and Jiang, 2007) climate models. In terms of precipitation, the pattern is dominated by drier conditions in most of the model domain. However, precipitation amount over the TP itself is mainly unaffected, except for an extensive increase in the southeastern part, which we assign to a model artefact. In general, precipitation changes are strongly superimposed by internal variability within the time slices. Despite the noticeable cooling tendency, the spatial arrangement of climate types during the LGM episode can hardly be distinguished from the present-day situation, mainly because atmospheric circulation is more or less unchanged.

The temperature effect during the MH period is minor compared with the other paleo-climatic time slices. A slight cooling of less than 1 °C prevails over most of Asia. Over the TP and northern India it reaches up to 3 °C. During summer, the extratropical part of the model domain experiences some warming by 1–2 °C. While this minor cooling tendency in REMO is consistent with the majority of temperature reconstructions in central and eastern Asia (cf. Bartlein et al., 2011; Braconnot et al., 2012), it disagrees with former modeling approaches for the MH period that suggest a slight warming (Zheng et al., 2004; Polanski et al., 2012; Harrison et al., 2014). Concerning precipitation, our model confirms the wetter conditions over the TP, northern India, eastern Asia and northern China as suggested by other authors (e.g. Zheng et al., 2004; Polanski et al., 2012; Saraswat et al., 2013). Dallmeyer et al. (2013) recently compared their MH simulation to another set of proxy data for the Asian monsoon region (cf. Wang et al., 2010) and also concluded that the modeled precipitation increase over the central TP and its southern slopes is well in line with available proxies. Yet, the precipitation changes hardly stand out from the internal variability within the MH time slice. The climate classification during the MH is also largely congruent with the one under present-day conditions.

The application of a uniform downscaling approach with an RCM using the same model domain, resolution and model physics allows for a direct comparison of climate change signals among all considered paleo-climatic episodes despite their basically different mechanisms and times scales of natural climate variability. This is unprecedented for the uplift, LGM and MH episodes considered here. Not surprisingly, the uplift process is associated with the largest temperature and precipitation response and shift of climate types, at least on the basis of the entire TP region. These regional-mean changes hardly differ between REMO and ECHAM5. In both models, the uplift mainly affects the high-elevation clusters over the TP. However, the disappearance of the arid climate types north of the TP in the 25% and 0% experiments is a feature that only occurs at higher resolution in REMO. Another interesting finding is that at the scale of individual clusters, i.e. regional climates, glacial and, to a lower extent, MH conditions can provoke climate anomalies in the same order of magnitude as the uplift process. This mainly pertains to the climate types in northern India and along the southern slopes of the Himalaya where orbital forcing appears to be as important as tectonic changes during the Cenozoic (cd. Prell and Kutzbach, 1992). On the TP itself, however, the changes imposed by surface uplift are substantially larger than the ones induced by orbital forcing.

Given the probably artificial winter precipitation increase during the LGM episode (Fig. 11c) and some minor discrepancies with former modeling approaches in terms of temperature signals during the MH period (cf. Zheng et al., 2004; Polanski et al., 2012; Harrison et al., 2014), some specific characteristics and shortcomings of the RCM REMO have to be discussed, although the model generally performs very well over the Central Asian domain. From our experience with REMO in other regions, the model is very sensitive to deficiencies in the oceanic boundary conditions and vegetation-related land surface characteristics (Paeth et al., 2005, 2009). This makes it prone to wrong surface boundary conditions for paleo-climatic episodes. In addition, REMO has a systematic cold bias over the highest mountain chains surrounding the TP that is related to an overestimation of snow coverage and a warm bias in the Central Asian plains where intensive irrigation takes place (Mannig et al., 2013). Ongoing work is dedicated to improve the model (see Section 6).

6. Conclusions

Our first objective pertained to the hypothesis that glacial versus interglacial boundary conditions can produce similar climate changes as the uplift process during the Oligocene-Miocene-Pliocene period (cf. Prell and Kutzbach, 1992). This hypothesis could only be confirmed with respect to some regionally confined climate types, especially to the south of the TP. However, at the scale of the entire region of the TP and adjacent areas, climate is clearly more sensitive to the uplift than to orbital forcing during the LGM and MH periods.

The second hypothesis referred to the added value of simulated high-resolution patterns of paleo-climatic states that are suitable for a quantitative comparison with climate reconstructions. For the LGM

period, this comparison is successful but based on a very small number of grid boxes. The proxy-data for the MH episode are more numerous and wide-spread over Asia (cf. Wang et al., 2010; Bartlein et al., 2011; Braconnot et al., 2012). However, they exhibit substantial uncertainty, drawing a picture of remarkable temperature rise and decrease at neighboring locations. In contrast, our model produces patterns of paleo-climatic anomalies that are spatially more coherent and physically consistent. Therefore, we suggest that RCMs are able to provide a valuable theoretical basis for the assessment of paleo-climate and the climatological interpretation of proxy-data.

In addition, we aimed at improving the spatiotemporal representation of paleo-climatic episodes in Asia. Indeed, the simulation periods of 12 to 40 years per time slice allowed for a sophisticated statistical analysis of climate changes in order to distinguish between real climate change signals and climate anomalies that do not stand out from internal variability. The horizontal resolution of 0.5° used in the RCM REMO has added value to the representation of climate across the TP, compared with the driving global climate model. This relates to the model bias in terms of present-day climate, the regional details of simulated climate patterns – especially for the cluster analysis – and some new insights into climate changes north of the TP, i.e. the appearance of the arid climate types in western China when the TP reaches at least 50% of its present-day elevation.

There is still room for improvement of the model itself, the modified boundary conditions and the number of experiments. First of all, the matrix of paleo-climatic simulations could be extended, accounting for spatially differentiated uplift scenarios (cf. Tapponnier et al., 2001; Tang et al., 2013a; Zhang et al., 2014), modified paleo-geography (Fluteau et al., 1999), and a decomposition of forcings during the LGM and MH periods (Liu et al., 2008a, 2008b; Polanski et al., 2012). This would lead to a more comprehensive understanding of the processes leading to paleo-climatic changes but, at the same time, require enormous computing resources beyond the scope of our project. In addition, simulations over several hundreds or thousands of years would help to assess the superposition of time scales of climate fluctuations and changes arising from internal and external sources of variability, respectively (cf. Lorenz and Lohmann, 2004).

The RCM REMO has been shown to have a good performance in terms of the prominent features of regional climate in Asia and on the TP. Some systematic biases can still be removed by statistical post-processing (e.g. Paeth, 2011). However, a major deficit is the simulation of precipitation over high-elevation lakes on the TP where surface water temperature in winter is substantially overestimated and precipitation amount by far too high. In the future, this problem will be tackled by implementing the lake model FLake (Mironov et al., 2010) in REMO. Some further improvements can be expected when REMO is used in a version that is fully coupled to an ocean model enhancing the physical consistency of the climate simulations (cf. Sein et al., 2015). Recently, Gao et al. (2015) have implemented a more realistic land cover classification in REMO and reported an enhanced skill of the model. Finally, the aspect of model uncertainty must be addressed also for the assessment of paleo-climatic changes, e.g. by running a multi-model ensemble of RCMs nested into different global climate models from the PMIP3 initiative. Combining this with the matrix of more sensitivity studies implies a significant computational effort that could be achieved in the framework of a potential future paleo-CORDEX initiative.

Acknowledgements

We thank the ECMWF, the NCAR-NCEP, the Climatic Research Unit and the Department of Climatology at Freie Universität Berlin for providing the ERA40 reanalyses, the NCEP reanalyses, the CRU data set and the High Asian Reanalysis (HAR), respectively. This work was supported by the German Research Foundation (DFG) grants PA 1194/7 and EH 329/2, and European Research Council (ERC) Consolidator Grant number 615703 to T. Ehlers.

References

Arnold, L., Bréon, F.-M., Brewer, S., 2009. The Earth as an extrasolar planet: the vegetation spectral signature today and during the last Quaternary climatic extrema. Int. J. Astrobiol. 8, 81.

Barthi, V., Singh, C., 2015. Evaluation of error in TRMM 3B42V7 precipitation estimates over the Himalayan region. J. Geophys. Res. 120, 12458–12473.

Bartlein, P.J., et al., 2011. Pollen-based continental climate reconstructions at 6 and 21 ka: a global synthesis. Clim. Dyn. 37, 775–802.

Bershaw, J., Penny, S.M., Garzione, C.N., 2012. Stable isotopes of modern water across the Himalaya and eastern Tibet: Implications for estimates of paleoelevation and paleoclimate. J. Geophys. Res. 117. https://doi.org/10.1029/2011JD016132.

Botsyun, S., Sepulchre, P., Risi, C., Donnadieu, Y., 2016. Impacts of Tibetan Plateau uplift on atmospheric dynamics and associated precipitation $\delta^{18}O$. Clim. Past 12. https://doi.org/10.519/cp-12-1401-2016.

Braconnot, P., Harrison, S.P., Kageyama, M., Bartlein, P.J., Masson-Delmotte, V., Abe-Ouchi, A., Otto-Bliesner, B., Zhao, Y., 2012. Evaluation of climate models using Palaeoclimatic data. Nat. Clim. Chang. 2, 417–424.

Clift, P.D., Plumb, R.A., 2008. The Asian Monsoon: Causes, History and Effects. Cambridge Univ. Press.

Clift, P.D., Tada, R., Zheng, H., 2014. Monsoon evolution and tectonics-climate linkage in Asia: an introduction. Geol. Soc. Lond. Special Publ. 342, 1–4.

Dallmeyer, A., Claussen, M., Wang, Y., Herzschuh, U., 2013. Spatial variability of Holocene changes in the annual precipitation pattern: a model-data synthesis for the Asian monsoon region. Clim. Dyn. 40, 2919–2936.

Dietrich, S., Werner, M., Spangehl, T., Lohmann, G., 2013. Influence of orbital forcing and solar activity on water isotopes in precipitation during the mid- and late Holocene. Clim. Past 9, 13–26.

Ehlers, T.A., Poulsen, C.J., 2009. Influence of Andean uplift on climate and paleoaltimetry estimates. Earth Planet. Sci. Lett. 281 (3–4), 238–248. https://doi.org/10.1016/j.epsl.2009.02.026.

Fluteau, F., Ramstein, G., Besse, J., 1999. Simulating the evolution of the Asian and African monsoons during the past 30 Myr using an atmospheric general circulation model. J. Geophys. Res. 104, 11995–12018.

Gao, Y., Weiher, S., Markkanen, T., Pietikänen, J.-P., Gregow, H., Henttonen, H.M., Jacob, D., Laaksonen, A., 2015. Implementation of the CORINE land use classification in the regional climate model REMO. Boreal Environ. Res. 20, 261–282.

Geng, Q., Wu, P., Zhao, X., Wang, Y., 2014. Comparison of classification methods for the division of wet/dry climate regions in Northwest China. Int. J. Climatol. 34, 2163–2174.

Grießinger, J., Bräuning, A., Helle, G., Thomas, A., Schleser, G., 2011. Quaternary Holocene Asian summer monsoon variability reflected by d18O in tree-ring from Tibetan junipers. Geophys. Res. Lett. 38, L03701.

Guangliang, H., Chongyi, E., Xiangjun, L., 2013. Reconstruction of integrated temperature series of the past 2000 years on the Tibetan Plateau with 10-year intervals. Theor. Appl. Climatol. 113, 259–269.

Guo, D., Wang, H., 2012. The significant climate warming in the northern Tibetan Plateau and its possible causes. Int. J. Climatol. 32, 1775–1781.

Hagemann, S., Dümenil Gates, L., 2003. Improving a subgrid runoff parameterization scheme for climate models by the use of high resolution data derived from satellite observations. Clim. Dyn. 21, 349–359.

Hahn, D.G., Manabe, S., 1975. The role of mountains in the South Asian monsoon circulation. J. Atmos. Sci. 32, 1515–1541.

Harrison, S.P., Bartlein, P.J., Brewer, S., Prentice, I.C., Boyd, M., Hessler, I., Holmgren, K., Itzumi, K., Willis, K., 2014. Climate model benchmarking with glacial and mid-Holocene climates. Clim. Dyn. 43, 671–688.

Insel, N., Poulsen, C.J., Ehlers, T.A., 2010. Influence of the Andes Mountains on South American moisture transport, convection, and precipitation. Clim. Dyn. 35 (7–8), 1477–1492. https://doi.org/10.1007/s00382-009-0637-1.

Insel, N., Poulsen, C.J., Ehlers, T.A., Sturm, C., 2012. Response of meteoric d18O to surface uplift – implications for Cenouoic Andean Plateau growth. Earth Planet. Sci. Lett. 317-318, 262–272.

IPCC, 2013. Climate Change 2013, the Physical Science Basis, Working Group I Contribution to the Fifth Assessment Report of the Intergovernmental Panel on Climate Change. Cambridge Univ. Press, Cambridge, pp. 1535.

Jacob, D., 2001. A note to the simulation of the annual and interannual variability of the water budget over the Baltic Sea drainage basin. Meteorog. Atmos. Phys. 77, 61–74.

Ju, L.H. Wang, Jiang, D., 2007. Simulation of the Last Glacial Maximum climate over East Asia with a regional climate model nested in a general circulation model. Palaeogeogr. Palaeoclimatol. Palaeoecol. 248, 376–390.

Jungclaus, J.H., Keenlyside, N., Botzet, M., Haak, H., Öuo, J.J., Latif, M., Marotzke, J., Mikolajewicz, U., Roeckner, E., 2006. Ocean circulation and tropical variability in the coupled model ECHAM5/MPI-OM. J. Clim. 19, 3952–3972.

Kalnay, E., Kanamitsu, M., Kistler, R., Collins, W., Deaven, D., Gandin, L.S., Iredell, M., Saha, S., White, G., Woolen, J., Zhu, Y., Chelliah, M., Ebisuzaki, W., Higgins, W., Janowiak, J., Mo, K.C., Ropelewsky, C., Wang, J., Leetma, A., Reynolds, R., Jenne, R., Joseph, D., 1996. The NCEP/NCAR 40-year Reanalysis Project. Bull. Am. Meteorol. Soc. 77, 437–471.

Kitoh, A., Motoi, T., Arakawa, O., 2010. Climate modelling study on mountain uplift and Asian monsoon evolution. Geol. Soc. Lond. Spec. Publ. 342, 293–301.

Kutzbach, J.E., Guetter, P.J., Ruddiman, W.F., Prell, W.L., 1989. Sensitivity of climate to Quaternary Cenozoic uplift in southern Asia and the American West: Numerical experiments. J. Geophys. Res. 94, 18393–18407.

Kutzbach, J.E., Prell, W.L., Ruddiman, W.F., 1993. Sensitivity of Eurasian climate to surface uplift of the Tibetan Plateau. J. Geol. 101, 177–190.
Le Pichon, X., Fournier, M., Jolivet, L., 1992. Kinematics, topography, shortening, and extrusion in the India-Eurasia collision. Tectonics 11, 1085–1098.
Li, J., Ehlers, T.A., Mutz, S., Steger, C., Paeth, H., Werner, M., Poulsen, C.J., Feng, R., 2016. Modern precipitation d18O and trajectory analysis over the Himalaya-Tibet orogen from ECHAM5-wiso simulations. J. Geophys. Res. 121, 10432–10452.
Li, J., Ehlers, T.A., Werner, M., Mutz, S., Steger, C., Paeth, H., 2017. Late Quaternary climate, precipitation d18O, and Indian Monsoon variations over the Tibetan Plateau. Earth Planet. Sci. Lett. 457, 412–422.
Liebke, U., Appel, E., Ding, L., Zhang, Q., 2013. Age constraints on the India-Asia collision derived from secondary remanences of Tethyan Himalayan sediments from the Tingri area. J. Asian Earth Sci. 62, 329–340.
Liu, X.D., Dong, B., 2013. Influence of the Tibetan Plateau uplift on the Asian monsoon-arid environment evolution. Chin. Sci. Bull. 58, 4277–4291.
Liu, X.D., Yin, Z.-Y., 2002. Sensitivity of East Asian monsoon climate to the Tibetan Plateau uplift. Palaeoclim. Palaeoecol. 183, 223–245.
Liu, Y., He, J., Li, W., Chen, L., 2008a. MM5 simulations of the China regional climate during the LGM. I: influence of CO_2 and Earth orbit change. Acta Meteorol. Sin. 22, 8–21.
Liu, Y., He, J., Li, W., Chen, L., 2008b. MM5 simulations of the China regional climate during the LGM. I: Influence of change of land area, vegetation, and large-scale circulation background. Acta Meteorol. Sin. 22, 22–30.
Liu, X.D., Guo, Q.C., Guo, Z.T., Yin, Z.-Y., Dong, B., Smith, R., 2015. Where were the monsoon regions and arid zones in Asia prior to the Tibetan Plateau uplift. Natl. Sci. Rev. 2, 403–416.
Liu, X.H., Xu, Q., Ding, L., 2016. Differential surface uplift: Cenozoic palaeoelevation history of the Tibetan Plateau. Sci. China Earth Sci. 59, 2105–2120.
Lorenz, S., Lohmann, G., 2004. Acceleration technique for Milankowitch type forcing in a coupled atmosphere-ocean circulation model: method and application for the Holocene. Clim. Dyn. 23, 727–743.
Ma, D., Boos, W., Kuang, Z., 2014. Effects of orography and surface heat fluxes on the South Asian summer monsoon. J. Clim. 27, 6647–6659.
Mannig, B., Müller, M., Starke, E., Merkenschlager, C., Mao, W., Zhi, X., Podzun, R., Jacob, D., Paeth, H., 2013. Dynamical downscaling of climate change in Central Asia. Glob. Planet. Chang. 110, 26–39.
Maussion, F., Scherer, D., Mölg, T., Collier, E., Curio, J., Finkelnburg, R., 2014. Precipitation seasonality and variability over the Tibetan Plateau as resolved by the High Asia Reanalysis. J. Clim. 27, 1910–1927.
Mironov, D., Heise, E., Kourzeneva, E., Ritter, B., Schneider, N., Terzhevik, A., 2010. Implementation of the lake parameterization scheme Flake into the numerical weather prediction model COSMO. Boreal Environ. Res. 15, 218–230.
Mischke, S., Wünnemann, B., Appel, E., 2013. Proxies for Quarternary monsoon reconstruction on the Tibetan Plateau. Quart. Int. 313-314 (1–2).
Mitchell, T.D., Jones, P.D., 2005. An improved method of constructing a database of monthly climate observations and associated high-resolution grids. Int. J. Climatol. 25, 693–712.
Molnar, P., 2005. Mio-Pliocene growth of the Tibetan Plateau and evolution of east African climate. Palaeontol. Electr. 8, 1–23.
Molnar, P., Rajagopalan, B., 2012. Quaternary Miocene upward and outward growth of eastern Tibet and decreasing monsoon rainfall over the northwestern Indian subcontinent since ~10 MA. Gephys. Res. Lett. 39, L09702.
Mutz, S.G., Ehlers, T.A., Li, J., Steger, C., Paeth, H., Werner, M., Poulsen, C.J., 2016. Precipitation d18O over the Himalaya-Tibet orogen from ECHAM5-wiso sImulations: Statistical analysis of temperature, topography, and precipitation. J. Geophys. Res. 121, 9278–9300. https://doi.org/10.1002/2016JD024856.
Mutz, S.G., Ehlers, T.A., Werner, M., Lohmann, G., Stepanek, C., Li, J., 2018. Estimates of late Cenozoic climate change relevant to Earth surface processes in tectonically active orogens. Earth Surf. Dyn. 6 (2), 271–301 10/gc8sbw.
Netzel, P., Stepinski, T., 2016. On using a clustering approach for global climate classification. J. Clim. https://doi.org/10.1175/JCLI-D-15-0640.1.
Paeth, H., 2011. Postprocessing of simulated precipitation for impact studies in West Africa – part I: model output statistics for monthly data. Clim. Dyn. 36, 1321–1336.
Paeth, H., Born, K., Podzun, R., Jacob, D., 2005. Regional dynamical downscaling over West Africa: Model evaluation and comparison of wet and dry years. Meteorol. Z. 14, 349–367.
Paeth, H., Born, K., Girmes, R., Podzun, R., Jacob, D., 2009. Regional climate change in tropical Africa under greenhouse forcing and land-use changes. J. Clim. 22, 114–132.
Paeth, H., Hall, N.M., Gaertner, M.A., Dominguez Alonso, M., Moumouni, S., Polcher, J., Ruti, P.M., Fink, A.H., Gosset, M., Lebel, T., Gaye, A.T., Rowell, D.P., Moufouma-Okia, W., Jacob, D., Rockel, B., Giorgi, F., Rummukainen, M., 2011. Progress in regional downscaling of West African precipitation. Atmos. Sci. Lett. 12, 75–82.
Paeth, H., Müller, M., Mannig, B., 2015. Global versus local effects on climate change in Asia. Clim. Dyn. 45, 2151–2164.
Park, H.-S., Chiang, J.C.H., Bordoni, S., 2012. The mechanical impact of the Tibetan Plateau on the seasonal evolution of the south Asian monsoon. J. Clim. 25, 2394–2407.
Paxian, A., et al., 2015. Bias reduction in decadal predictions of West African monsoon rainfall using regional climate models. J. Geophys. Res. https://doi.org/10.1029/2015JD024143.
Polanski, S., Rinke, A., Dethloff, K., 2012. Simulation and comparison between mid-Holocene and preindustrial Indian summer monsoon circulation using a regional climate model. Open Atmos. Sci. J. 6, 42–48.
Poulsen, C.J., Ehlers, T.A., Insel, N., 2010. Onset of convective rainfall during Gradual late Miocene rise of the Central Andes. Science 328 (5977), 490–493. https://doi.org/10.1126/science.1185078.
Prell, W.L., Kutzbach, J.E., 1992. Sensitivity of the Indian monsoon to forcing parameters and implications for its evolution. Nature 360, 647–652.
Rayner, N.A., Horton, E.B., Parker, D.E., Folland, C.K., Hackett, R.B., 1996. Version 2.2 of the global sea ice and sea surface temperature data set, 1903-1994. In: Clim. Res. Tech. Note CRTN74. Bracknell, Hadley Centre.
Rowley, D.B., Currie, B.S., 2006. Palaeo-altimetry of the late Eocene to Miocene Lunpola basin, Central Tibet. Nature 439, 677–681.
Ruddiman, W.F., 2014. Earth's Climate. Past and Future. W.H. Freeman and Company, New York.
Saeed, F., Hagemann, S., Jacob, D., 2011. A framework for the evaluation of the South Asian summer monsoon in a regional climate model applied to REMO. Int. J. Climatol. 32, 430–440.
Saraswat, R., Nigam, R., Correge, T., 2013. A glimpse of the Quaternary monsoon history from India and adjoining seas. Palaeogeogr. Palaeclimatol. Palaeoecol. 397, 1–6.
Sein, D.V., Mikolajewicz, U., Gröger, M., Fast, I., Cabos, W., Pinto, J.G., Hagemann, S., Semmler, T., Izquierdo, A., Jacob, D., 2015. Regionally coupled atmosphere-ocean-sea ice-marine biogeochemistry model ROM: 1. Description and validation. J. Adv. Model. Earth Syst. 7, 268–304.
Song, J.-H., Kang, H.-S., Byun, Y.-H., Hong, S.-Y., 2009. Effects of the Tibetan Plateau on the Asian summer monsoon: a numerical case study using a regional climate model. Int. J. Climatol. 30, 743–759.
Su, F., Duan, X., Chen, D., Cuo, L., 2013. Evaluation of the global climate models in the CMIP5 over the Tibetan Plateau. J. Clim. 26, 3187–3208.
Tang, H., Micheels, A., Eronen, J., Ahrens, B., Fortelius, M., 2013a. Asynchronous responses of East Asian and Indian summer monsoons to mountain uplift shown by regional climate modeling experiments. Clim. Dyn. 40, 1531–1549.
Tang, H., Eronen, J., Micheels, A., Ahrens, B., 2013b. Strong interannual variation of the Indian summer monsoon in the Quaternary Miocene. Clim. Dyn. 41, 135–153.
Tapponnier, P., Xu, Z.Q., Roger, F., Meyer, B., Arnaud, N., Wittlinger, G., Yang, J.S., 2001. Oblique stepwise rise and growth of the Tibet Plateau. Science 294, 1671–1677.
Uppala, S., et al., 2005. The ERA-40 re-analysis. Q. J. R. Meteorol. Soc. 131, 2961–3012.
Wang, T., Hong, D., Jahn, B., Tong, Y., Wang, Y., Han, B., Wang, X., 2006. Timing, petrogenesis, and setting of Paleozoic synorogenic intrusions from the Altai mountains, northwest China: implications for the tectonic evolution of an accretionary orogen. J. Geol. 114, 735–751.
Wang, Y., Liu, X., Herzschuh, U., 2010. Asynchronous evolution of the Indian and east Asian summer monsoon indicated by Holocene moisture patterns in monsoonal central Asia. Earth Sci. Rev. 103, 135–153.
Werner, M., Langebroek, P.M., Carlsen, T., Herold, M., Lohmann, G., 2011. Stable water isotopes in the ECHAM5 general circulation model: toward high-resolution isotope modeling on a global scale. J. Geophys. Res. 116. https://doi.org/10.1029/2011JD015681.
Wilks, D.S., 2006. Statistical Methods in the Atmospheric Sciences. Academic Press, Amsterdam (627pp).
Windley, B.F., Allen, M.B., 1993. Mongolian Plateau: evidence for a late Cenozoic mantle under Central Asia. Geology 21, 295–298.
Wu, G., Liu, Y., Dong, B., Liang, X., Duan, A., Bao, Q., Yu, J., 2012. Revisiting Asian monsoon formation and change associated with Tibetan Plateau forcing: I, Formation. Clim. Dyn. 39, 1169–1181.
Yang, T., Hao, X., Shao, Q., Xu, C.-Y., Zhao, C., Chen, X., Wang, W., 2012. Multi-model ensemble projections in temperature and precipitation extremes of the Tibetan Plateau in the 21st century. Glob. Planet. Chang. 80 (81), 1–13.
Zhang, R., Jiang, D., Zhang, Z., Yu, E., 2014. The impact of regional uplift of the Tibetan Plateau on the Asian monsoon climate. Palaeogeogr. Palaeoclimatol. Palaeoecol. 417, 137–150.
Zheng, Y.Q., Yu, G., Wang, S.M., Xue, B., Zhuo, D.Q., Zeng, X.M., Liu, H.Q., 2004. Simulation of paleoclimate over East Asia at 6 ka BP and 21 ka BP by a regional climate model. Clim. Dyn. 23, 513–529.